Galvanic Displacement Across Single-Layer Graphene

by

Isabelle Cunitz

Bachelor of Science in Environmental Engineering
University of Oklahoma, 2019

Submitted to the Department of Mechanical Engineering
in Partial Fulfillment of the Requirements for the Degree of

Master of Science

at the

Massachusetts Institute of Technology

September 2023

Authored by: Isabelle Cunitz
Department of Mechanical Engineering
August 25, 2023

Certified by: Rohit N. Karnik
Department of Mechanical Engineering
Thesis Supervisor

Accepted by: Nicolas Hadjiconstantinou
Graduate Officer, Department of Mechanical Engineering

Galvanic Displacement Across Single-Layer Graphene

by

Isabelle Cunitz

Submitted to the Department of Mechanical Engineering on August 25, 2023
in Partial Fulfillment of the Requirements for the Degree of Master of Science

ABSTRACT

This work aims to advance the scientific and engineering understanding of galvanic displacement reactions as buffered by a monolayer of graphene, specifically by investigating palladium deposition on graphene on a copper foil substrate via galvanic displacement between the copper and palladium (II) ions in solution. To understand palladium nanoparticle deposition and determine how this process can be controlled, electrochemical thermodynamics and classical nucleation theory are first synthesized into a thermodynamic model of the system. Next, scanning electron microscopy is used to characterize palladium deposition on the graphene/copper surface after galvanic displacement. Copper etch pits are observed to form during the reaction, maintaining contact between the deposition solution and the copper and thereby ensuring that the reaction is not self-limiting under the conditions studied. Palladium is observed to preferentially deposit along atomic steps in the copper foil, at graphene defects where the copper is exposed to the deposition solution, and at etch pits. The effects of varying palladium concentration and graphene/copper surface treatments are characterized, and these results are synthesized to propose a mechanism of palladium deposition via galvanic displacement through graphene. Finally, galvanic displacement is investigated in a novel engineering application, as a method of sealing graphene defects for the synthesis of centimeter-scale nanoporous atomically thin membranes. Palladium nanoparticles deposited on the graphene surface are observed to largely survive graphene transfer to a support membrane substrate, as well as mounting and use in aqueous diffusion cell experiments. However, diffusion experiments show that graphene treated via galvanic displacement has higher leakage than untreated graphene, indicating that under the reaction conditions studied here, galvanic displacement has a net effect of graphene defect enhancement rather than defect sealing. This work contributes new insights regarding galvanic displacement as a method of modifying monolayer graphene, as well as exploring this method in the novel application of membrane separations. With further development, this simple, quick, and inexpensive technique for the fabrication of 2D material/nanoparticle composites may have a myriad of possible applications relevant to medicine, sustainability, and beyond.

Thesis supervisor: Rohit N. Karnik
Title: Tata Professor, Department of Mechanical Engineering

Acknowledgements

This material is based upon work supported by the National Science Foundation Graduate Research Fellowship under Grant No. 2141064.

I want to first thank my advisor, Rohit Karnik, for his guidance and insight, and for welcoming me into his lab. I also thank all of my colleagues at the Karnik Lab at MIT, especially the graphene team. In particular, thank you to Lohyun Kim for providing the Python script used to interpret diffusion test data in this work.

I thank all my friends in Boston and beyond; my sister Ronnie and brother Greg; and Alex and Tasha for all the support, distraction, and love.

Finally, thank you to my incredible parents, Wendy Marx-Cunitz and Ron Cunitz, for everything.

Table of contents

List of figures

1. Introduction

1.1. Motivation

Engineering and science at the smallest physical scales can be instrumental to addressing the world's largest, most complex challenges. In the two decades since the isolation of graphene in 2004[1], a family of diverse two-dimensional (2D) materials has emerged, attracting intense research interest due to their exciting physical, chemical, and electrical properties. 2D materials functionalized or otherwise modified with nanostructures have a range of applications relevant to diverse fields, from biomedicine to sustainability and beyond. Typically synthesized with techniques such as electrodeposition, electroless deposition, and hydrothermal synthesis, nanocomposites of 2D materials with nanoparticles of metals, metal oxides, and other materials have been studied for use in applications including biomedical imaging and theraputics[2]; electrochemical biomolecule detection[3,4]; aqueous and gas-phase sensing[3,5]; energy conversion and storage[6,7]; and catalysis, including hydrolysis and CO_2 conversion[6].

This thesis intends to advance the understanding of galvanic displacement as a facile and versatile method of fabricating nanostructures on 2D materials. The deposition of palladium on single-layer graphene via galvanic displacement between palladium ions in solution and the graphene's copper substrate is studied, with palladium being a relevant material for catalysis, sensing, and hydrogen storage applications[8,9] and graphene being the prototypical 2D material with a host of superior physiochemical properties[10].

This study aims to both elucidate the mechanisms of palladium nanoparticle deposition in this system and explore the knobs available to tune the deposition process, including reaction conditions, palladium concentration, and graphene pre-treatment. By developing and applying a conceptual model informed by electrochemical thermodynamics and classical nucleation theory, experimental results are connected to the underlying physics to understand how and where the nanoparticles are fabricated on the graphene surface. Furthermore, practical use of

the palladium-decorated graphene is explored. Its robustness to handling is investigated, and it is used for the first time in the application of nanoporous atomically thin membranes.

1.2. Literature review

1.2.1. Corrosion

Galvanic reactions, or spontaneous reduction-oxidation reactions driven by differences in reduction potential between materials, have been thoroughly studied for hundreds of years. The physicist Alessandro Volta, who discovered in 1800 the production of electric current by dissimilar metals connected by an electrolyte[11], coined the term galvanism to describe this phenomenon, in tribute to his contemporary Luigi Galvani and his famous experiments using electricity to reanimate frogs' legs[12,13].

In a modern context—besides batteries, where the reduction and oxidation reactions are separated and harnessed for electric power—galvanism is typically understood in the context of corrosion. Corrosion, or the process of metal degradation via oxidation in the environment, has been estimated to cost 3-4% of a nation's gross domestic product[14], and much effort has been devoted to alleviating its effects. Broadly speaking, corrosion is fundamentally thermodynamically favorable, as metals experience a strong driving force to return to their native oxide state[15]. Typically, corrosion mitigation strategies focus on slowing the kinetics of this degradation rather than attempting to alter the thermodynamics, with strategies including applying protective coatings, exploiting natural oxide layers (such as the extremely thin protective oxide film formed on aluminum), and sacrificial anodization (such as the zinc applied to make galvanized steel)[15,16].

1.2.2. Galvanic displacement for nanofabrication

Recently, far from the typical understanding of galvanic reactions as destructive, researchers have exploited this class of reactions as an electroless deposition technique for nanofabrication. In the context of nanofabrication, galvanic displacement proceeds as follows: Noble metal ions in solution are reduced on the surface of a substrate with a lower reduction potential, while the substrate is simultaneously oxidized. This process is typically limited by the formation of a layer of the deposited metal[17,18] or a layer of the substrate's oxide[19], protecting the surface of the substrate from the deposition solution (see Figure 1).

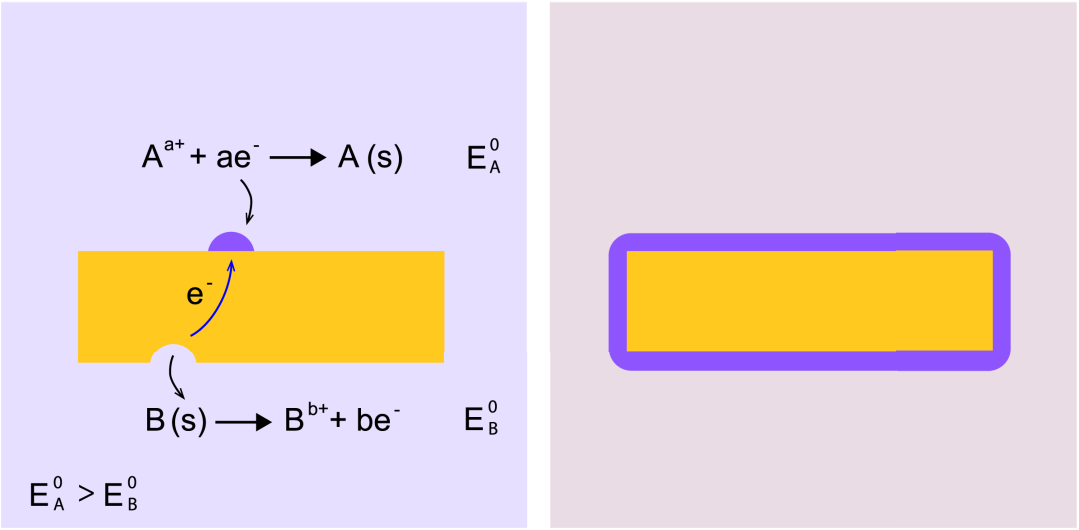

Figure 1. Galvanic displacement for deposition of metal nanostructures on a substrate. This reaction is driven by differences in reduction potential between the species in solution (E_A) and the solid substrate (E_B) and is limited by the deposition solution's access to the substrate.

Galvanic displacement has attracted much research interest in the past two decades as a technique for creating metal nanostructures, largely for the fabrication of semiconductors and catalysts. This technique is extremely simple (not requiring chemical reducing agents as in other electroless deposition techniques, an external current source as in electrodeposition, or complex instrumentation), quick under ambient lab conditions, cost-effective, and versatile[17,18,19,20,21,22,23,24,25,26,27,28]. Diverse metal nanostructures, such as films, disks, belts,

particles, and dendrites, can be achieved by carefully adjusting the galvanic displacement reaction conditions; in a systematic analysis of the reaction between a copper nanoparticle substrate and silver ions in solution, Liu and Sen showed that a high cell potential tends to result in kinetic control and (in extreme cases) dendrite-type deposition, while conditions closer to equilibrium result in thermodynamic control and film-type deposition[28]. Beyond its facile and versatile nature, galvanic displacement exhibits several additional advantages. It is highly selective to the substrate and can closely conform the deposited metal to complex geometries (for example, to pattern semiconductor surfaces or fabricate extended surface catalysts)[17,22,29,30]; it is advantageous for fabricating bimetallic or alloyed nanostructures[20,29,31,32]; it can be tuned to produce films with good mechanical properties (such as strong adhesion to the substrate)[17,19,23,30]; and it can form self-limited and even epitaxial layers under the correct conditions[19,23,24,33].

Galvanic displacement can be controlled by adjusting the cell potential of the relevant reduction-oxidation reaction, i.e. by changing the composition of the substrate or the composition or concentration of the ion in solution. However, galvanic displacement's primary disadvantage, compared to other nanofabrication techniques, is that tight control of the morphology of the deposited nanostructures can be difficult to achieve, in part due to how quickly the reaction progresses once the substrate is exposed to the deposition solution[17,18,22]. Interfacial defects or impurities such as step edges in the substrate typically have a high level of impact on the deposition reaction and the deposited metal's morphology[17,34]. Furthermore, while metals deposited via galvanic displacement can exhibit advantageous mechanical and structural properties, this is dependent on the ion-substrate pair and the reaction conditions and is not observed in all cases. Structures deposited via galvanic displacement have exhibited mechanical failure[35], poor adhesion to the substrate[27,30], and unwanted oxides at the structure-substrate interface[22,23]. In order to fully benefit from the advantages of galvanic displacement for fabricating metal nanostructures, it is necessary to engineer the system to achieve as much control as possible over the reaction.

1.2.3. Galvanic reactions and 2D materials

Galvanic reactions through 2D materials have largely been studied in the context of assessing 2D coatings for metal corrosion mitigation. 2D materials are theoretically good candidates for corrosion mitigation coatings because of their thinness, strength, and impermeability, but defects from the growth and transfer processes can compromise their effectiveness by creating pathways for oxidizing species to access the substrate[36]. Much of the research in this space has focused on graphene, the prototypical 2D material since its isolation in 2004[1].

Much optimism initially surrounded graphene as a corrosion mitigation coating; promising results demonstrated corrosion mitigation of metals coated with chemical vapor deposition-grown graphene monolayers[37,38,39,40,41,42] and coatings derived from reduced graphene oxide powder[43,44,45], with the coating effectively isolating the metal from its environment. However, graphene's electrically conductive nature means that it easily promotes localized corrosion at any scratches or hole-type defects that expose the metal to its environment, in addition to graphene itself being cathodic to many metals[36,45,46,47,48]. Alternate 2D materials, particularly less electrically conductive ones such as hexagonal boron nitride or molybdenum disulfide, may therefore be better situated as coatings to suppress galvanic reactions[36,49,50].

In contrast to corrosion, metal nanostructure fabrication via galvanic displacement through 2D materials is much less well understood. While researchers have exploited galvanic displacement between an ion in solution and the 2D material itself to deposit nanoparticles on nanoflakes of molybdenum disulfide[51] and made composite catalysts via galvanic displacement between dissimilar metals, both supported by a substrate of reduced graphene oxide powder[32,52], only a few studies explicitly explore galvanic displacement as buffered by a layer of a 2D material separating the substrate and the ion in solution.

Ho et al. utilized galvanic displacement between chemical vapor deposition-grown graphene's copper substrate and gold ions in a chloroauric acid solution to deposit gold nanoparticles along

cracks and bare patches in the graphene's surface[53]. In addition to the crack-filling effect achieved by a direct galvanic displacement reaction between gold ions and the exposed copper, they observed a few nanoparticles deposited on the graphene surface between cracks, which they attribute to a separate, slower reaction between the gold ions and the graphene itself. However, this explanation fails to take into account the excellent electrical conductivities of both graphene and copper. The researchers transferred the gold-decorated graphene from the copper substrate with a polymer-assisted transfer technique and ultimately used the material as a transparent electrode for solar cells, taking advantage of its improved sheet resistance due to the crack filling effect.

Hong et al. published two studies exploring galvanic displacement through 2D materials in more detail, specifically within a palladium/graphene/copper model system. This group decorated graphene with palladium via galvanic displacement by submerging graphene on copper in a solution of palladium chloride and sodium chloride, with their proposed reaction mechanism indicating oxidation from the underside of the copper to support the reduction of palladium into nanoparticles or nanolayers on the graphene surface[54,55]. FE-SEM and TEM imaging were used to characterize the resulting palladium deposition patterns, and graphene defects were identified as crucial to palladium nanoparticle nucleation below a posited critical concentration, above which palladium would deposit in a homogeneous layer over the graphene surface[55]. They identified several types of defects at which the palladium preferentially deposited: graphene grain boundaries, graphene wrinkles, line-shaped formations identified as fatigue cracks in the copper substrate, and areas where the CVD had produced multiple graphene layers[55]. Raman analysis was used to argue that the galvanic displacement reaction produced minimal damage to the structure of the graphene itself[54,55]. The group exploited palladium's hydrogen-absorbing properties, specifically the change in sheet resistance of the palladium-decorated graphene upon exposure to hydrogen gas, to build a hydrogen sensor[54] and used the improved sheet resistance of the palladium-decorated graphene to make a transparent and flexible heater device[55].

The effectiveness of galvanic displacement between ions in solution and graphene's copper substrate for decorating the graphene with nanoparticles has been established by this prior work. However, the mechanisms of these reactions have not yet been fully elucidated, and open questions include how to control deposition and what other applications may be promising for graphene prepared with this nanofabrication technique.

1.3. Model system

This study concerns the galvanic displacement between palladium (II) ions in solution and copper foil through a centimeter-scale single layer of graphene.

Palladium is a favorable material for a wide range of catalysis applications, including hydrogenation, oxidation, organic coupling, and reactions relevant to different types of fuel cells[8,9]. Being more abundant on Earth than the typically used electrocatalyst platinum, palladium is a more cost-effective material[9], and nanoparticles' high surface area to volume ratio make them particularly effective for catalysis[8]. Furthermore, palladium's ability to adsorb hydrogen makes it ideally situated for hydrogen sensing, separations, and storage applications relevant to the hydrogen economy[8,9].

Graphene's extraordinary physiochemical properties, including its Young's modulus of 1 TPa, strength of 130 GPa, flexibility, optical transparency, high electrical and thermal conductivities, impermeability to gases, and readiness to functionalization, make it an exciting material for any number of applications[10].

Nanoparticles of palladium and palladium alloys synthesized on powders of two-dimensional graphene-related materials such as reduced graphene oxide have been demonstrated on the benchtop scale for catalyzing oxidation reactions[56,57,58], oxygen reduction[59], and organic synthesis[60], as well as enabling hydrogen storage[61] and glucose sensing[62,63] applications.

Copper is a convenient reducing agent for the galvanic displacement reaction, as graphene is commonly commercially manufactured via chemical vapor deposition (CVD) on a copper foil substrate due to copper's low cost and low carbon solubility[64,65].

The principles explored by studying this palladium/graphene/copper model system are relevant to other systems in which galvanic displacement occurs through single-layer graphene.

1.4. Research questions

This thesis aims to address two broad questions.

Firstly, to advance the scientific understanding of galvanic displacement through graphene: In what morphologies are the palladium nanoparticles deposited, and how can this process be controlled?

Secondly, to apply this nanofabrication technique in a novel engineering context: Can this galvanic displacement reaction be exploited to improve transport through graphene as a membrane material?

2. Materials and methods

2.1. Materials

All graphene used in this study was CVD-grown monolayer graphene on copper foil manufactured by Graphenea[65]. When directly comparing nanoparticle deposition between samples, every effort was made to use graphene from the same batch to eliminate the effects of between-batch inconsistencies in graphene quality. In this study, when graphene is from a different batch in side-by-side comparisons, this is explicitly noted. All samples of graphene on copper, with and without palladium nanoparticles, were stored in a vacuum chamber at < 17 kPa when not actively in use for experiments or imaging to minimize oxidation of the copper foil.

Palladium (II) chloride was 99% purity (Sigma-Aldrich) and sodium chloride was ACS reagent grade, ≥ 99.0% purity (Sigma-Aldrich). Two molecular weights of poly(methyl methacrylate) (PMMA) were used in the polymer-assisted graphene transfer process, 15 kDa (Sigma-Aldrich) and 495 kDa (Kayakli), both dissolved in anisole. Ammonium persulfate used for copper etching was APS Copper Etchant 100 (Transene). Potassium chloride used for diffusion tests was BioUltra grade (Sigma-Aldrich).

For the transport experiments, ipPORE^{TM} polyimide track etched membranes manufactured by It4Ip were used as support membranes, with pore diameter 20 nm, pore number density 6 x 10^9 / cm^2, and thickness 8 μm[66].

All water used in this study was ultrapure (type 1) deionized (DI) water at 18.2 MΩ·cm resistivity from the Direct-Q® 3 UV water purification system (Millipore)[67].

2.2. Methods

2.2.1. Palladium deposition

A stock solution of 5 mM $PdCl_2$ and 0.15 M NaCl (pH = 4.35) was prepared, and various dilutions of this solution were used for deposition. Palladium was deposited via galvanic displacement by either submerging the graphene on copper in the deposition solution (typically 5 or 20 mL) or by applying a droplet of the deposition solution (typically 20 µL) to the surface of the graphene on copper in a closed Petri dish, in the presence of a Kimwipe wet with DI water to minimize evaporation. After nanoparticle deposition, each sample was rinsed three times by submerging in DI water for five minutes, and subsequently air dried in the ambient lab environment. This rinsing procedure was intended to ensure that no excess $PdCl_2$ or NaCl from the deposition solution contaminated the surface of the graphene during sample analysis.

2.2.2. Scanning electron microscopy

All scanning electron microscopy (SEM) micrographs for this work were collected using a Zeiss Merlin high-resolution scanning electron microscope at 1-3 kV accelerating voltage, 100 pA current, and 3-4 mm working distance. Conductive samples (i.e. graphene on copper) were affixed to the metal SEM stub with nonconductive tape at the corners to minimize damage to the samples, while nonconductive samples (i.e. graphene transferred to a PI membrane support) were affixed to the stub with conductive carbon tape to maximize electron flow for imaging.

2.2.3. Image analysis

Number densities and size ranges of nanoparticles were obtained by counting by hand and comparing pixel numbers to SEM scale bars, within 1 μm^2 or 9 μm^2 areas of raw SEM images,

using the Adobe Illustrator software[68]. Therefore, all nanoparticle number densities and size ranges presented in this work are approximate and represent data from a small part of the sample, and are thus useful for rough comparison purposes only. While the author attempted to automate nanoparticle extraction from SEM images, this proved to be difficult due to the small size of the nanoparticles and the presence of background features in the images, such as copper atomic step edges. Further image analysis was conducted using the OpenCV computer vision library in the Python programming language[69,70].

2.2.4. Graphene transfer

Graphene was transferred to the polyimide support membranes using a polymer-assisted transfer process. Briefly, centimeter-scale samples of graphene on copper foil were spincoated with three layers of the 15 kDa PMMA and one layer of the 495 kDa PMMA. Typically in the transfer process, the samples were then briefly floated on 100% APS to remove any material on the bottom of the copper foil. However, it was discovered that the samples that were treated via submersion in the deposition solution were weakened, and the copper foil crumpled after even brief treatment with 100% APS. Therefore, this step was skipped for samples that had been deposited with palladium nanoparticles via submersion.

The samples were next floated on diluted APS overnight to slowly etch away the copper foil. After floating on DI water to remove residual APS, the samples were scooped from beneath with the polyimide support membrane, which had been pre-treated with brief oxygen plasma exposure to improve its hydrophilicity. The samples were then left to dry, after which the PMMA support layer was dissolved by submerging the samples in acetone and isopropanol.

2.2.5. Plasma treatment

Plasma treatment was conducted using a Harrick Plasma PDC-001 expanded plasma cleaner with PlasmaFlo gas mixer[71] on the lowest plasma intensity setting. Oxygen used during plasma treatment was ultra high purity 100% compressed oxygen (Airgas).

2.2.6. Focused ion beam treatment

Focused ion beam milling was done using an FEI Helios Nanolab 600 Dual Beam System, with gallium ions at 30 kV voltage, 9.7 pA current, and 1 µs dwell time. In silicon multipass milling mode, a grid of cylindrical volumes from 10 nm to 1 µm in diameter and 0.1 nm to 200 nm in depth was programmed to be milled out of the graphene/copper surface.

2.2.7. Diffusion testing

For the transport tests, 7 mL PermeGear Side-Bi-Side glass diffusion cells with a 4.78 mm orifice diameter were used[72]. Membranes were mounted between the feed and permeate sides using silicone gaskets and pre-treated with ethanol to ensure full wetting for the diffusion tests. After the wetting treatment, 6 mL of 0.5 M KCl and 6 mL of DI water were simultaneously introduced to the feed side and permeate side, respectively. Conductivity on the permeate side was monitored using a Mettler Toledo SevenCompact conductivity meter[73] to obtain the concentration of KCl over time as it diffused through the membrane from the feed side to the permeate side. During all diffusion tests, both sides were well-stirred with magnetic stir bars at 800 rpm to minimize boundary layer effects at the membrane interfaces. Diffusion test conductivity data were converted into membrane permeance values using a Python script.

3. Understanding palladium deposition

3.1. Thermodynamic theory

3.1.1. Electrochemical reaction

Neglecting any side reactions, the standard cell potential of the galvanic displacement reaction can be found using the standard reduction potentials of palladium (II) and copper:

$$Pd^{2+} + 2e^- \rightarrow Pd\ (s) \qquad E^0 = 0.951\ V\ \ vs.SHE\ ^{74}$$

$$Cu\ (s) \rightarrow Cu^{2+} + 2e^- \qquad E^0 = 0.3419\ V$$

$$Pd^{2+} + Cu\ (s) \rightarrow Pd\ (s) + \ Cu^{2+} \qquad E^0_{cell} = 0.6091\ V$$

To prepare the deposition solutions used in this study, $PdCl_2$ is dissolved in an excess of NaCl, as $PdCl_2$ is well known to be insoluble in water but soluble in chloride solutions[75]. The actual speciation of the palladium is partitioned between $PdCl_4^{2-}$, $PdCl_3^-$, hydroxopalladium, and mixed chlorohydroxopalladium complexes, depending on NaCl concentration and pH[76,77], and is unlikely to include the Pd^{2+} ion itself in significant concentrations. The assumption that the Pd^{2+} ion is reduced in the reaction with the copper substrate for thermodynamic modeling purposes is in line with the larger galvanic displacement for nanofabrication literature, which often neglects detailed speciation considerations in favor of simplified models that use standard ion reduction potentials[9,20,22,23,26,29,30,51,55,78].

The Nernst equation can then be used to model the reaction driving force under non-standard conditions. Assuming activities of unity for solid palladium and copper and taking the activities of the dissolved species to be their concentrations:

$$E_{cell} = E^0_{cell} + \frac{RT}{nF}\ln\left(\frac{\prod_{reactants} {a_i}^{\nu_i}}{\prod_{products} {a_i}^{\nu_i}}\right) \quad (1)$$

$$= 0.6091\ V + \frac{RT}{2F}\ln\left(\frac{[Pd^{2+}]}{[Cu^{2+}]}\right) \quad (2)$$

where a_i = activity of species i

ν_i = reaction quotient of species i

R = gas constant, 8.3145 $\frac{J}{mol \cdot K}$

T = temperature

n = number of electrons transferred in the reaction

F = Faraday's constant, 96,485 $\frac{C}{mol}$

This can be converted to the Gibbs free energy of reaction:

$$\Delta G_{rxn} = -nFE_{cell} \quad (3)$$

$$= \Delta G^0_{rxn} - RTln\left(\frac{\prod_{reactants} {a_i}^{\nu_i}}{\prod_{products} {a_i}^{\nu_i}}\right) \quad (4)$$

$$= -117.54\ \frac{kJ}{mol} - RTln\left(\frac{[Pd^{2+}]}{[Cu^{2+}]}\right) \quad (5)$$

This simple model provides insight into how the reaction driving force scales with the concentrations of the species involved.

3.1.2. Classical nucleation theory

In addition to this favorable electrochemical driving force, there are surface energies associated with nanoparticle formation that oppose the introduction of a new solid species in contact with the deposition solution and substrate. Classical nucleation theory is a framework that is commonly used to conceptualize these opposing energies, but it had not before this study been applied to nanoparticle deposition via galvanic displacement across 2D materials.

Pioneered by Volmer and Weber[79] and Becker and Döring[80], among others, classical nucleation theory is used to model the kinetics of the nucleation of new phases, both homogeneous[81,82]

and heterogeneous[83,84,85]. This approach involves several assumptions that limit the predictive power of first-principles calculations, including the major assumption that the properties (bulk and surface energies) of substances at the sub-nanometer scale of the nucleus are the same as their macroscopic properties. This assumption breaks down at very small nucleus sizes[86]. Nucleation rates are extremely sensitive to small changes to these molecular-scale energies, as well as to other factors such as temperature and the presence of impurities[81,86]. Therefore, experimental data are typically fit to classical nucleation theory models to find effective surface energy values, rather than using the models for first-principles nucleation rate predictions[83,84,85,87]. Nonclassical approaches, such as using density functional theory to predict molecular-scale energies, modeling diffuse interfaces between the nucleus and the bulk phase, and modeling multistep nucleation, can update the classical model to reflect the underlying physics of nucleation more accurately and therefore get closer to experimental results[86,88].

For the purposes of this study, the classical nucleation theory framework is used to understand the competing energies associated with nanoparticle formation, and qualitative agreement is reached between this framework and the experimental results. A detailed study of the nucleation kinetics of the palladium/graphene/copper model system, including the fitting of experimental data to the classical nucleation theory model to obtain effective surface energies, is left to future work.

For general nanoparticle nucleation on a substrate submerged in a fluid, the Gibbs free energy of nanoparticle formation can be modeled by the following expression:

$$\Delta G_{NP} = V_n \Delta g + A_{nf}\gamma_{nf} + A_{ns}(\gamma_{ns} - \gamma_{fs}) \quad (6)$$

where V_n = nanoparticle volume

$\Delta g = \frac{\Delta G_{rxn}}{V_m}$ = Gibbs free energy of reaction per unit volume

V_m = molar volume of nanoparticle material

A_{nf} = contact area between nanoparticle and fluid

A_{ns} = contact area between nanoparticle and substrate

γ_{nf}, γ_{ns}, γ_{fs} = interfacial energies between nanoparticle material (*n*), fluid (*f*), and substrate (*s*)

In the palladium/graphene/copper galvanic displacement system explored in this study, copper is being dissolved at the same time as the palladium deposits, resulting in the formation of etch pits in the copper which presumably provide some surface energy contribution due to the increase in area of the substrate-fluid interface. In this analysis, surface area changes due to substrate dissolution are neglected for simplicity, and also with the consideration that the etch pits are large in size relative to the palladium nanoparticles and therefore provide a smaller surface energy contribution. While this assumption is not entirely physical, it is acceptable for the purpose of this analysis, which is to understand the basic energy competition underlying nanoparticle deposition. Due to classical nucleation theory's inherent limitations as discussed above, it is often most helpful for such basic arguments rather than for developing detailed models of particle nucleation.

Further assuming that the particles are hemispherical, again for simplicity,

$$\Delta G_{NP} = \frac{2}{3}\pi r^3 \Delta g + \pi r^2 (2\gamma_{nf} + \gamma_{ns} - \gamma_{fs}) \quad (7)$$

$$= \Delta G'_{rxn} + \Delta G_{surface} \quad (8)$$

where *r* = nanoparticle radius

The overall Gibbs free energy of nanoparticle formation can therefore be decomposed into two contributions. The free energy of the electrochemical reaction, $\Delta G'_{rxn}$, which scales with the nanoparticle volume, is opposed by the free energy associated with interfacial energies, $\Delta G_{surface}$, which scales with the nanoparticle surface area (see Figure 2). It should be noted that $\Delta G'_{rxn}$ has units of energy, in contrast to ΔG_{rxn}, the free energy change of the reaction on a per mole basis.

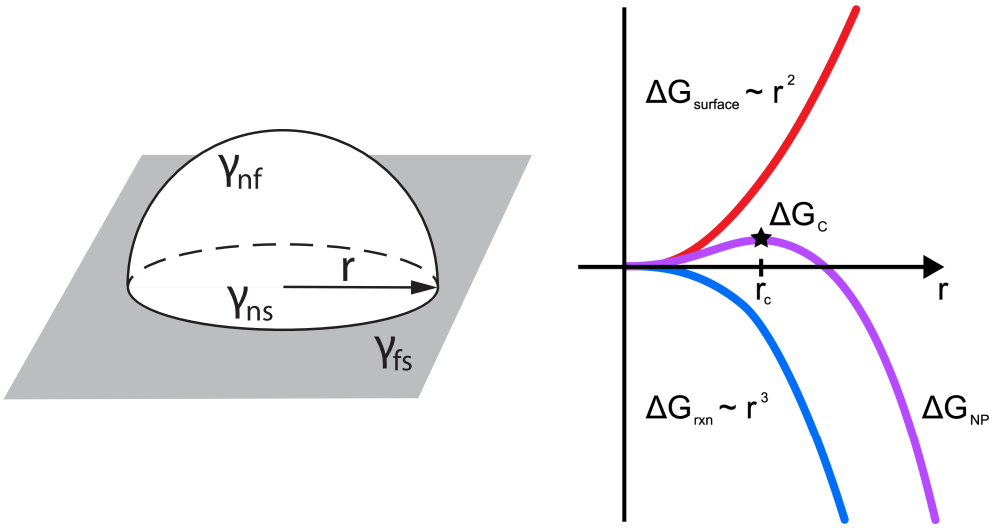

Figure 2. Hemispherical nanoparticle schematic and free energy dependence on radius.

Therefore, nanoparticle nucleation can be understood as an activated-type process. For a nanoparticle below a certain critical size, the adverse surface energies will dominate and the nanoparticle will tend to dissolve back into solution. Once a nanoparticle reaches the critical size, however, the favorable driving force of the reaction will dominate and it will tend to survive: the nucleation event is successful. The critical radius can be found by setting the derivative of ΔG_{NP} with respect to r equal to zero; for this geometry,

$$r_c = -\frac{2\gamma_{nf} + \gamma_{ns} - \gamma_{fs}}{\Delta g} \tag{9}$$

where r_c = critical radius for nanoparticle nucleation

The nucleation rate is exponentially related to the Gibbs free energy of nanoparticle formation at the critical radius, or activation energy,

$$\Delta G_c = \frac{\pi}{3}\frac{\left(2\gamma_{nf} + \gamma_{ns} - \gamma_{fs}\right)^3}{\Delta g^2} \tag{10}$$

$$\frac{dN}{dt} = Ae^{-\frac{\Delta G_c}{k_B T}} \tag{11}$$

where $\Delta G_c = \Delta G_{NP}(r_c)$, activation energy of nanoparticle nucleation

$N = N(t)$, number of nucleated nanoparticles over time

A = pre-exponential factor

k_B = Boltzmann constant, 1.38 x 10^{-23} $\frac{J}{K}$

More favorable thermodynamics, from a more negative $\Delta G'_{rxn}$ or more favorable $\Delta G_{surface}$ (see Equations 7 and 8), correspond to a smaller critical radius and lower activation energy, and therefore faster nucleation at a given temperature.

In this system, $\Delta G'_{rxn}$ can be modulated by adjusting the concentrations of the species in the deposition solution, in accordance with Equation 5. $\Delta G_{surface}$ can be expected to be more favorable at features on the graphene/copper substrate that have a higher interfacial energy with the deposition solution. Substrate defects, such as atomic step edges, grain broundaries, and point vacancies, are known to encourage heterogeneous nucleation due to such surface energy effects[82,89].

3.2. Graphene features

Typical features and defects of the as-purchased graphene/copper matrix as observed by SEM are shown in Figure 3, including graphene wrinkles, multiple graphene layers from CVD that proceeded slightly too far, SiO_2 contamination from the quartz CVD tube in the form of bright nanoscale particles embedded in the surface, and grain boundaries and atomic steps in the underlying copper foil[90,91,92]. Smaller graphene defects, such as grain boundaries or point vacancies of the carbon lattice, are in all likelihood present but would not be visible via SEM imaging.

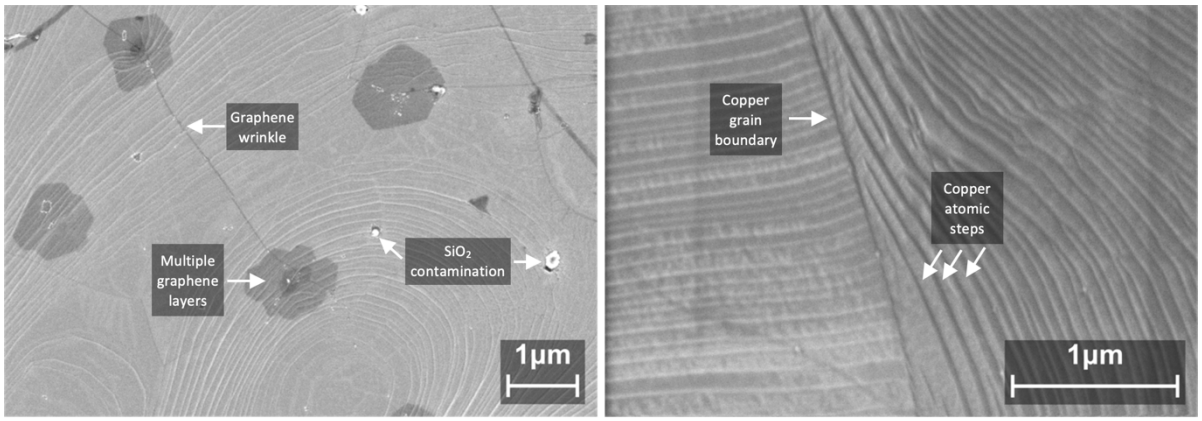

Figure 3. Unaltered, commercially grown graphene on copper. Features visible include graphene wrinkles, patches of multiple graphene layers, SiO_2 contamination, a copper foil grain boundary, and copper atomic steps. Images are from different graphene batches.

3.3. Effect of limiting contact

Unaltered CVD-grown graphene on copper exhibits both hole-type and non-hole-type features and defects. In previous studies with this system, palladium nanoparticles were deposited on the graphene surface by submerging the graphene on copper in the deposition solution. Nanoparticles were observed depositing preferentially not just on graphene holes directly exposing copper to the deposition solution, but also on features such as graphene wrinkles, graphene grain boundaries, edges of areas with multiple graphene layers, and copper fatigue cracks; copper dissolved from the exposed underside of the foil[55]. For separations-focused defect sealing applications, however, the relevant features upon which to deposit nanoparticles are graphene holes, including both intrinsic hole-type defects from the CVD process (such as point vacancies and holes resulting from SiO_2 contamination) and larger graphene scratches associated with handling.

To better understand the factors controlling galvanic displacement through graphene and investigate the possibility of depositing palladium at only the hole-type graphene defects, where the graphene blocking the deposition solution's access to the copper substrate is

physically missing, different reaction conditions were tested. The galvanic displacement reaction was conducted by submerging centimeter-scale graphene on copper in the deposition solution and by applying a 20 μL droplet of the deposition solution to the surface of the graphene. For the droplet reaction, the deposition solution could only access the copper substrate through hole-type defects in the graphene, whereas the intent for the submerged reaction was to expose the deposition solution to the same area of copper foil (on the bottom of the sample) as graphene-covered copper (on the top).

Two competing hypotheses were proposed. For the droplet reaction, either nanoparticles would largely be deposited at hole-type defects and the reaction would be limited by their sealing, or the copper would be etched aggressively enough from initial holes that etch pits would form that keep the deposition solution in contact with copper. In this scenario, electrons would flow to support deposition at non-hole-type features of the graphene.

The SEM imaging results support this second hypothesis (see Figure 4). Large, micron-scale etch pits control deposition, with nanoparticles deposited in similar morphologies between the two samples. Unexpectedly, however, under these reaction conditions, etch pits are also observed on the submerged sample. This had not been reported in previous studies, in which graphene on copper was also submerged in the deposition solution.

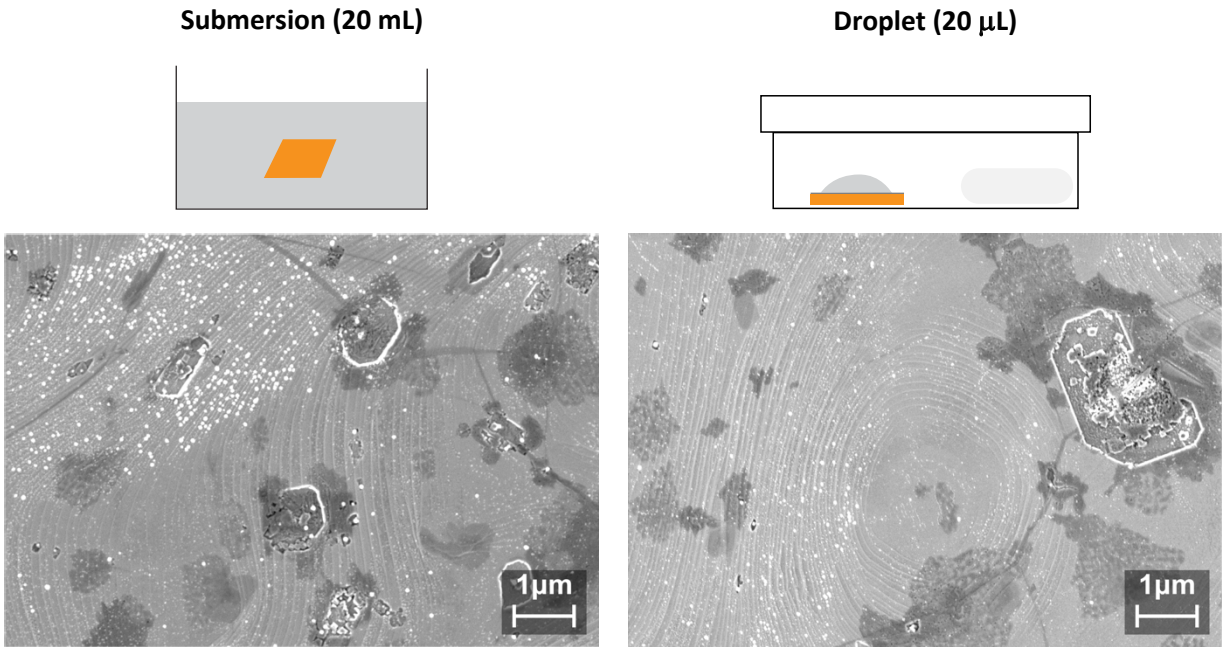

Figure 4. Effect of submerging graphene on copper in deposition solution vs. applying a small droplet. Palladium nanoparticles are visible as white dots on the graphene surface. Irregular, dark areas are likely copper oxide. Etch pits are visible in both the droplet sample (keeping the deposition solution in contact with the copper) and the submerged sample. 20 mL submersion (left) vs. 20 μL droplet (right) 0.1 mM $PdCl_2$ + 3 mM NaCl, 5 min reaction time.

Further investigating the presence of these etch pits in the submerged sample, both sides of a submerged sample were imaged. Features associated with graphene coverage, such as graphene wrinkles and areas of multiple layers of graphene, were present on both sides of this sample, along with palladium nanoparticles and etch pits. Therefore, the commercially-manufactured single-layer graphene on copper used for this study actually has a layer of graphene on both sides of the copper foil, and both the submerged and droplet samples are in fact in a regime of limited contact between the deposition solution and the copper substrate.

To observe the system's behavior when more copper is exposed to the deposition solution, graphene was physically wiped off of approximately half of one side of a graphene on copper sample before palladium deposition to expose a large stretch of the underlying copper to the deposition solution. The part of this sample covered with graphene, far from the exposed

copper region, also exhibited micron-scale etch pits (see Figure 5). While further study of palladium deposition with graphene on one side fully removed is warranted to repeat the results of Hong et al.[55], these results suggest that under these reaction conditions, exposure of the deposition solution to large areas of the copper substrate is not necessarily enough to stop the formation of etch pits.

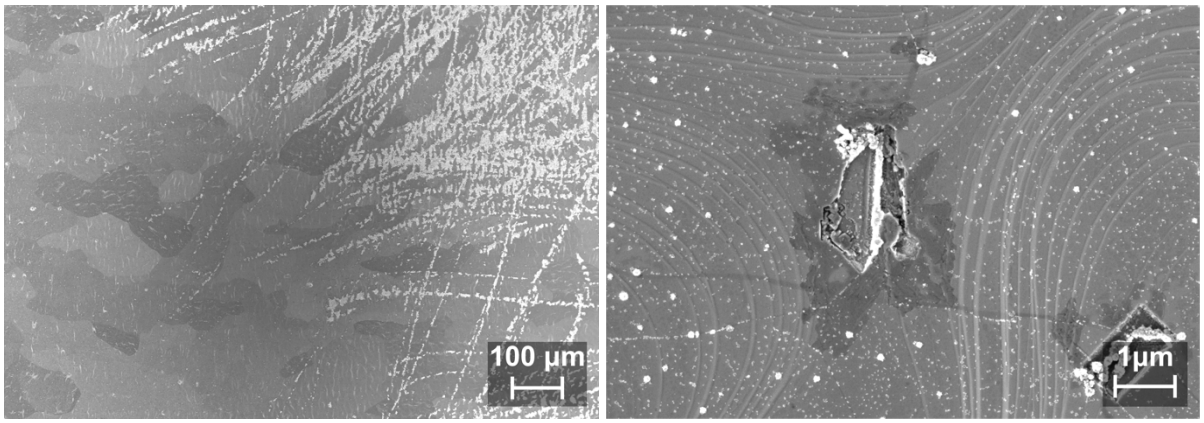

Figure 5. Palladium deposition on graphene on copper with area of graphene removed prior to deposition. Palladium deposited on the scratches, visible as bright lines in the SEM image (left); palladium deposition morphology, including copper etch pit, in area far from graphene-removed region (right). 5 mL submersion 0.1 mM $PdCl_2$ + 3 mM NaCl, 5 min reaction time.

As a whole, these results indicate that when the deposition solution's access to the copper substrate is limited, the reaction rectifies this via the formation of micron-scale etch pits in the copper. In this limited contact regime, etch pits are therefore crucial to controlling nanoparticle deposition. However, even when the deposition solution's access to the copper substrate is not totally limited by graphene, the reaction can be aggressive enough to form copper etch pits, thereby damaging the graphene layer that had originally been at the location of the etch pits.

3.4. Preferential nucleation observations

When depositing palladium on graphene via galvanic displacement with the copper substrate, nanoparticle deposition is typically inhomogeneous across the graphene/copper surface. As predicted by the thermodynamic framework, surface energy effects at certain features of the graphene or copper make these features more favorable for nanoparticle deposition than perfect stretches of graphene on copper.

In previous work with this system, features that promote nanoparticle nucleation were identified as wrinkles, cracks, and grain boundaries in the graphene, as well as edges of extra graphene layers[55]. In this study, certain features tended to exhibit preferential palladium deposition (see Figure 6).

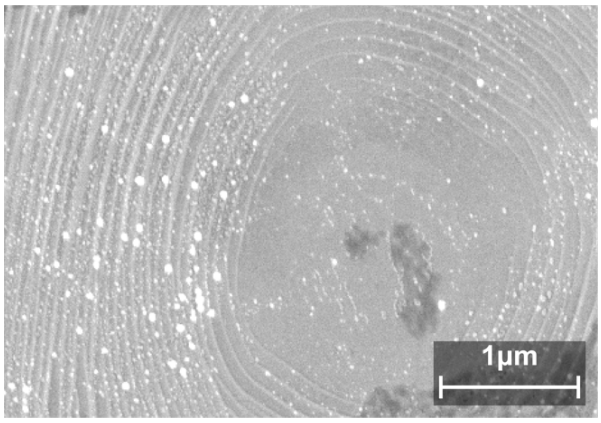

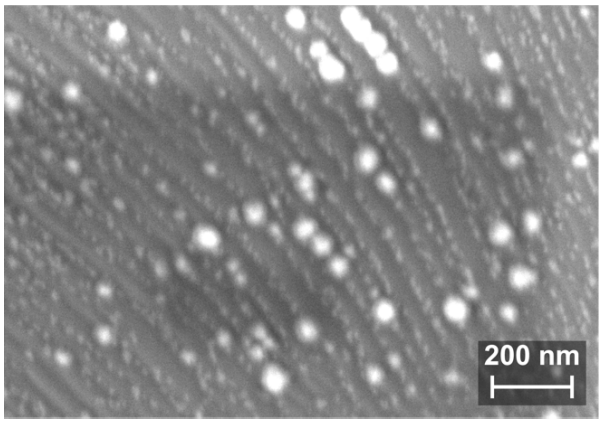

Copper foil atomic steps

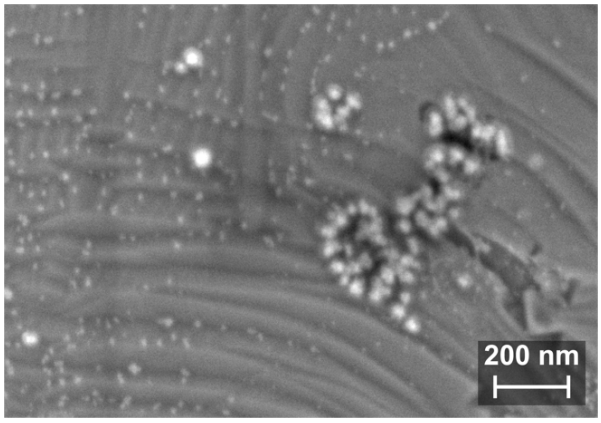

Graphene holes

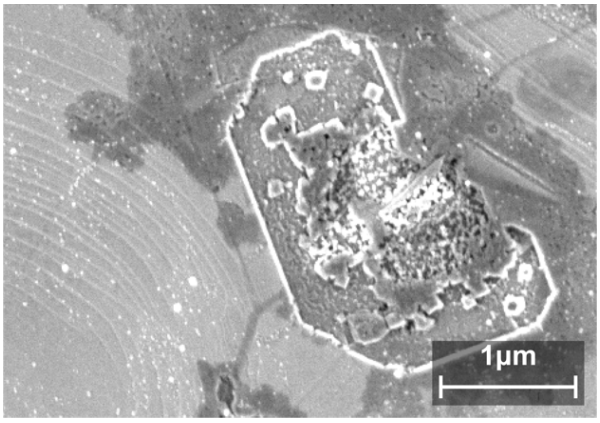

Copper etch pits

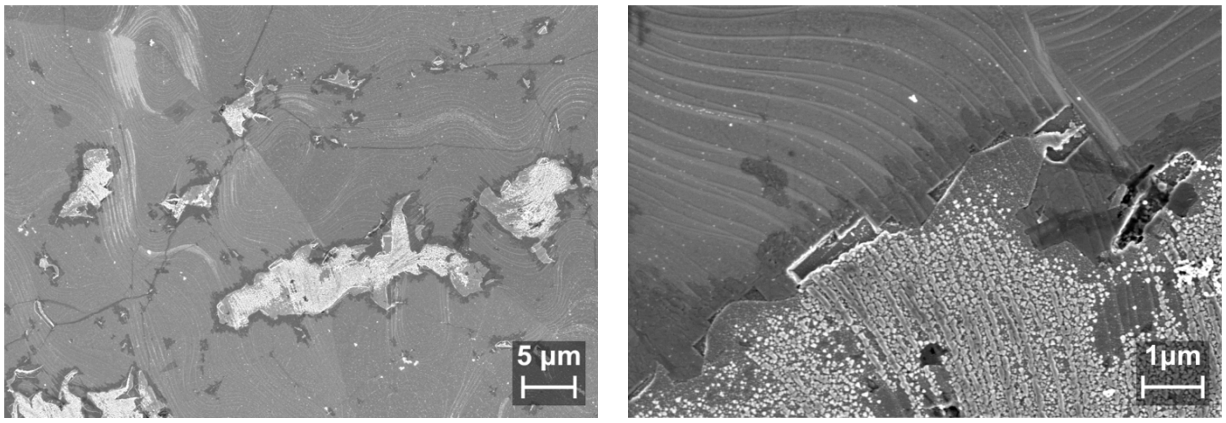

Figure 6. Preferential palladium nucleation patterns. Some images are from different graphene batches and reaction conditions, but all were 0.1 mM $PdCl_2$ + 3 mM NaCl, 5 min reaction time.

Not only are nanoparticles observed in greater densities in areas where copper atomic steps are closer together, the nanoparticles can be observed to follow the lines of the atomic steps. Nanoparticles can also be observed decorating holes in the graphene, such as holes from SiO_2 contamination during the CVD graphene fabrication process and even copper etch pits that are themselves a result of the galvanic displacement reaction. When the surface of a sample of graphene on copper was purposefully wiped with a Kimwipe to remove the graphene prior to nanoparticle deposition, palladium preferentially deposited to fill patches where graphene was removed. This type of deposition was also observed in another sample that was not intentionally damaged, indicating that it had been unintentionally scratched prior to palladium deposition.

Some of these results align with prior studies of galvanic displacement through single-layer graphene on its copper substrate. In particular, preferential deposition at areas where the deposition solution was in direct contact with the copper was reported both by Ho et al. for gold deposition[53] and Hong et al. for palladium deposition[54,55]. However, no evidence was found of selective deposition at the edges of multiple graphene layers or at wrinkles, as had been previously reported. Furthermore, no polygonal deposition patterns at the scale of several microns were observed, which Hong et al. had observed and attributed to deposition at

graphene grain boundaries[55]. A truly non-contact-limited regime, with graphene fully removed from one side of the copper prior to submersion, may be needed to replicate these results. There are also differences between the graphene used in this study and that used in previous work—for example, Hong et al. purposefully adjusted the CVD process to synthesize graphene with many wrinkles[55]—which are likely to alter selective deposition patterns.

3.5. Effect of varying concentration

The thermodynamics of the electrochemical reaction were next adjusted by changing the concentration of the palladium deposition solution over three orders of magnitude. As changes in the free energy of reaction are expected to scale with the log of the palladium (II) ion concentration as described in Equation 5, by changing the $PdCl_2$ concentration, the reaction driving force is altered. Since it was shown that the submersion and droplet methods yielded similar deposition patterns, these experiments were conducted with the droplet method for efficient use of the palladium solution.

The results range from sparse nanoparticle coverage at 0.01 mM $PdCl_2$ to a complete nanostructured layer of palladium over the graphene/copper surface at 5 mM (see Figure 7).

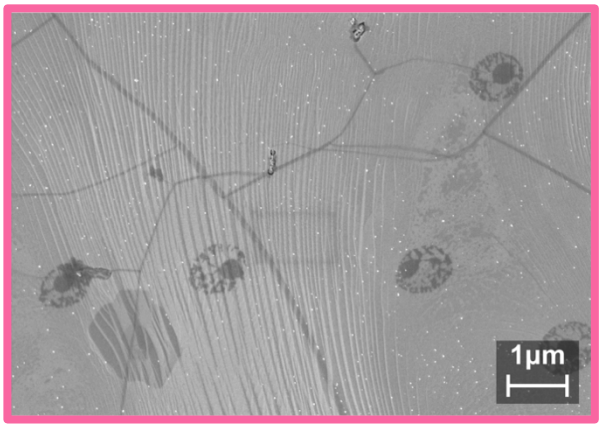

0.01 mM $PdCl_2$
ΔG_{rxn} ≈ -123 kJ/mol

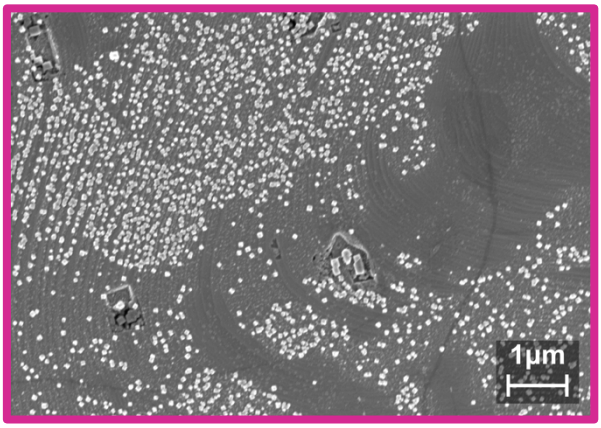

0.1 mM $PdCl_2$
ΔG_{rxn} ≈ -129 kJ/mol

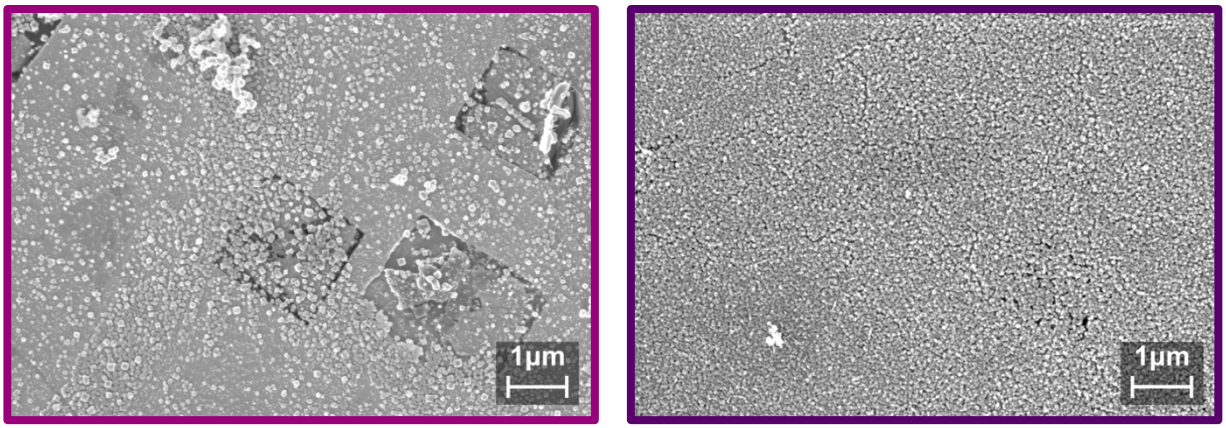

1 mM $PdCl_2$

ΔG_{rxn} ≈ -135 kJ/mol

5 mM $PdCl_2$

ΔG_{rxn} ≈ -139 kJ/mol

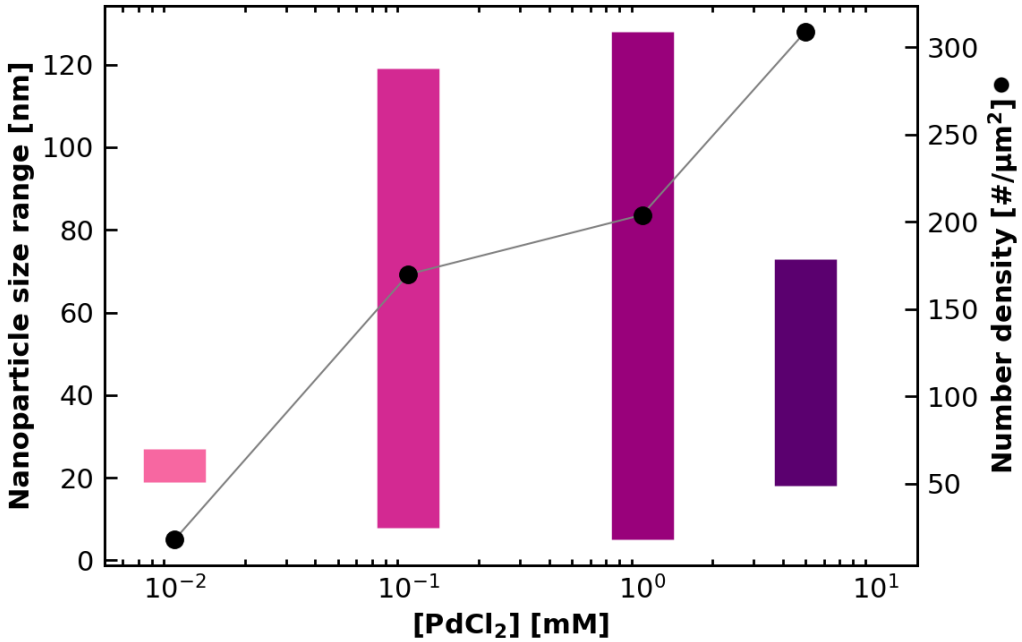

Figure 7. Effect of reaction driving force, modulated via deposition solution palladium concentration, on nanoparticle deposition (0.01, 0.1, 1, and 5 mM $PdCl_2$). ΔG_{rxn} estimated with Equation 5, with T = 25 °C, taking $[Pd^{2+}] = [PdCl_2]_{added}$ and making the standard assumption that $[Cu^{2+}] = 10^{-6}\ M$ [16]. Nanoparticle size (diameter) ranges and number densities obtained from analysis by hand of 1 µm² areas of SEM images; these values are therefore approximate (see Section 2.2.3 for details of image analysis methods). 20 µL droplet 0.01 – 5 mM $PdCl_2$ + 30x concentration NaCl, 5 min reaction time.

According to Equation 9, the critical radius of nanoparticle formation should decrease with an increased driving force of the reaction. The smallest nanoparticles observed decrease in size with greater palladium concentration until the entire surface is covered at 5 mM $PdCl_2$, corresponding to a smaller critical radius of formation. Furthermore, the largest nanoparticles similarly increase in size with greater palladium concentration, excluding the 5 mM data point, indicating faster nanoparticle growth during the 5 min reaction time. Approximate nanoparticle number density increases with greater palladium concentration, reflecting a higher nucleation rate as predicted by Equation 11.

Overall, these results qualitatively support the basic relationships between energies and nanoparticle nucleation as predicted by the framework of classical nucleation theory.

3.6. Effect of surface treatment

3.6.1. Oxygen plasma

Plasma is a commonly used tool for graphene modification, introducing defects and/or doping the graphene and thereby altering its physiochemical properties. Hui et al. found that when graphene is still attached to its copper CVD substrate during oxygen plasma exposure, a synergistic oxidation process occurs; oxidation of the copper through graphene defects happens simultaneously with graphene modification, prolonging the graphene's survival[93]. With increasing plasma exposure time, the graphene first experiences oxygen doping (the formation of epoxides, enolates, and hydroxides); the copper then scavenges oxygen atoms from these functional groups to support its own oxidation, which proceeds in conjunction with graphene damage until eventually the graphene is totally removed from the substrate in the form of carbon dioxide[93].

To investigate the effects of graphene surface treatment on palladium deposition, samples of graphene on copper were briefly exposed to O_2 plasma in a plasma chamber prior to the

galvanic displacement reaction (see Section 2.2.5 for details of plasma treatment). It should be noted that exposure to plasmas of nitrogen and air is much harsher on copper-supported graphene than exposure to O_2 plasma due to physical sputtering effects[94]. It is likely that some air contaminated the chamber during O_2 plasma treatment, somewhat decreasing the amount of protection that copper oxidation afforded the graphene via the mechanism described above.

SEM images of the palladium-decorated graphene on copper after galvanic displacement following various amounts of oxygen plasma pre-treatment are shown in Figure 8.

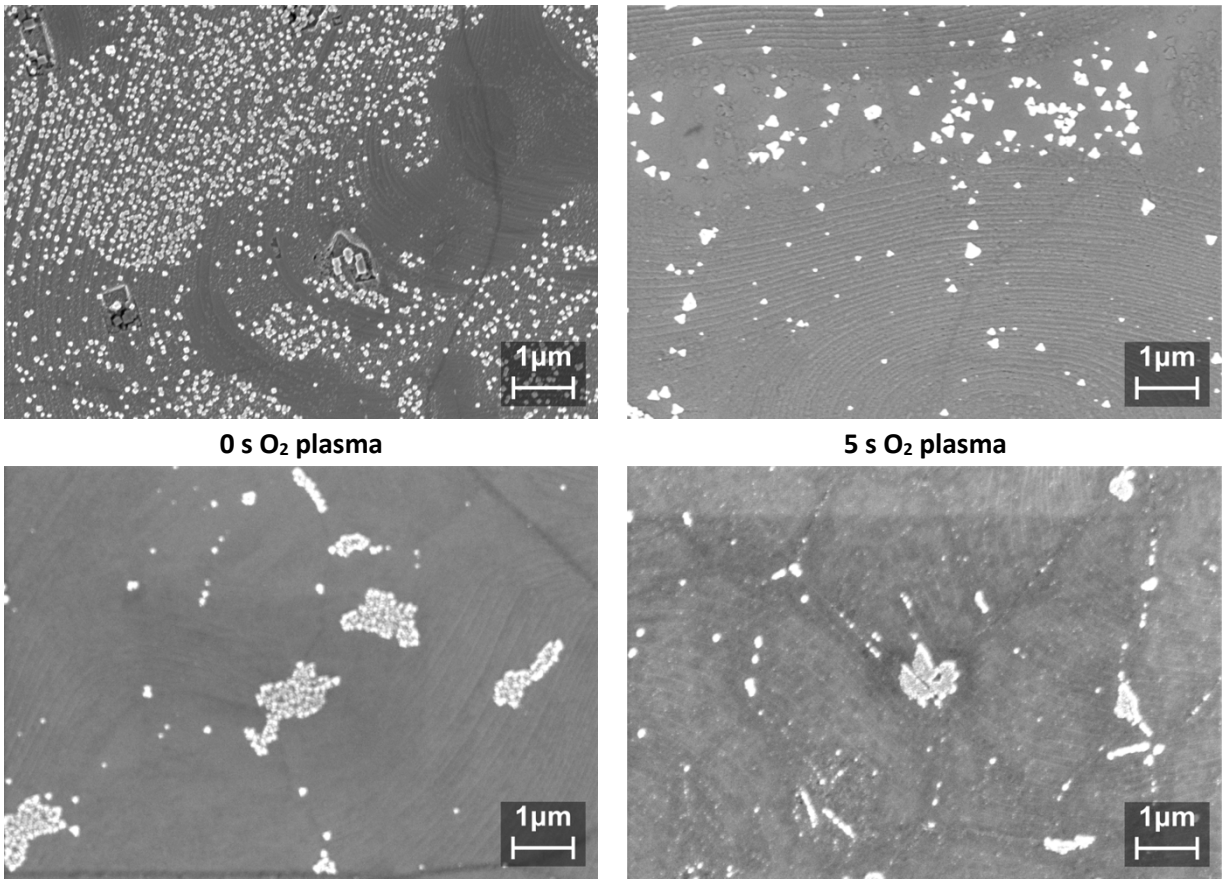

0 s O_2 plasma **5 s O_2 plasma**

10 s O_2 plasma **20 s O_2 plasma**

Figure 8. Palladium deposition after graphene/copper pre-treatment with O_2 plasma exposure (0, 5, 10, and 20 s). 0 s sample is from a different graphene batch than the others. 20 µL droplet 0.1 mM $PdCl_2$ + 3 mM NaCl, 5 min reaction time.

With 5 s of O_2 plasma pre-treatment, palladium was deposited as fewer and larger nanoparticles when compared to galvanic displacement on untreated graphene. While galvanic displacement after 0 s of O_2 plasma pre-treatment yielded roughly 170 nanoparticles per μm^2, between 8 and 119 nm in diameter (see Figure 7), galvanic displacement after 5 s of pre-treatement yielded 6 nanoparticles per μm^2, between 27 and 255 nm in diameter (from analysis by hand of a 9 μm^2 region of the image). Furthermore, they were not observed to align with the atomic steps of the underlying copper, and copper etch pits were not observed. When the plasma pre-treatment time was increased to 10 s, these large nanoparticles were observed to cluster in ~1 μm regions, with a few nanoparticles deposited on the graphene surface between clusters. Similarly to the 10 s O_2 plasma sample, the 20 s sample also showed ~1 μm clusters of palladium nanoparticles, but more nanoparticles were observed between the clusters, and evidence of copper oxidation beneath the graphene layer was pronounced (dark mottling in the SEM image).

These results broadly agree with the mechanism of graphene/copper modification by O_2 plasma as reported by Hui et al.[93] Nucleation being thermodynamically favorable at sites of chemical reactivity on the graphene surface and at exposed copper, palladium tends to deposit both at locations where the graphene is modified with functional groups and at locations where the graphene is removed. If the graphene functional groups formed during the initial stage of oxygen plasma exposure are mobile and tend to agglomerate, this would explain the formation of progressively larger regions of palladium deposition between 0, 5, and 10 s of O_2 plasma exposure. In the 20 s sample, nanoparticles are distributed over more of the graphene/copper surface, perhaps corresponding to progressive graphene damage after initial surface functionalization.

The darkening of the copper observed in the 20 s sample does not appear to be due to direct oxidation of the copper by the O_2 plasma, since it was only visible on the portion of the copper/graphene that was exposed to the droplet of the deposition solution. This may instead be due to greater oxidation of the copper during galvanic displacement, exacerbated by

damage done to the graphene during plasma treatment. The absence of copper etch pits in all of the plasma-treated samples is not fully explained but may be because of greater access of the deposition solution to the copper substrate due to graphene damage during plasma treatment, as compared to samples that received no plasma treatment prior to nanoparticle deposition.

3.6.2. Focused ion beam milling

Focused ion beam (FIB) milling with gallium ions was also investigated as a surface treatment prior to palladium nanoparticle deposition. A grid of cylindrical volumes, with diameters ranging from 10 nm to 1 µm and depths from 0.1 nm to 200 nm, was attempted to be milled from the graphene/copper surface before the galvanic displacement reaction (see Section 2.2.6 for detailed FIB milling methods). While the intent was to remove the graphene layer and underlying copper in a controlled manner to assess how the palladium deposited in the presence of such defects, the method did not work as expected. The graphene/copper surface did appear to be damaged by the FIB treatment, but cylinders of controlled dimensions were not milled into the surface. Visible holes in the copper were observed at higher gallium doses (larger programmed cylinder diameter and/or depth), but the holes were not cylindrical and were larger in diameter than they had been programmed to be.

Furthermore, SEM imaging after galvanic displacement showed that palladium was in fact largely blocked from being deposited near the sites where FIB milling had been done. A halo of little to no palladium deposition was observed around sites of FIB milling, with the effect being more pronounced at higher gallium doses (see Figure 9).

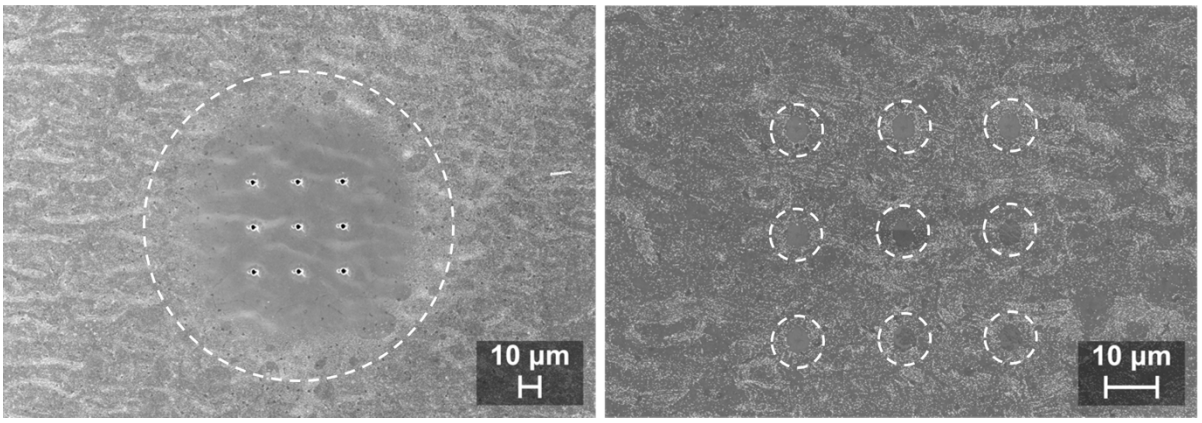

Figure 9. Palladium deposition after FIB pre-treatment, showing larger areas of little to no palladium deposition with higher gallium dose. Where a 3x3 grid of cylinders 1000 nm in diameter and 100 nm in depth was programmed to be milled, leading to visible holes in the copper/graphene, a large halo can be observed surrounding the grid (left, outlined by dashed circle). The site where a 3x3 grid of cylinders 200 nm in diameter and 10 nm in depth was programmed to be milled had a smaller halo around each point where the gallium ions had been directed (right). Submerged in 0.1 mM $PdCl_2$ + 3 mM NaCl, 5 min reaction time.

3.7. Proposed deposition mechanisms

Synthesizing these observations, a detailed mechanism of nanoparticle deposition via galvanic displacement through graphene can be proposed when a graphene/copper surface exhibiting some hole-type and non-hole-type features is exposed to a palladium deposition solution through the graphene layer (see Figure 10).

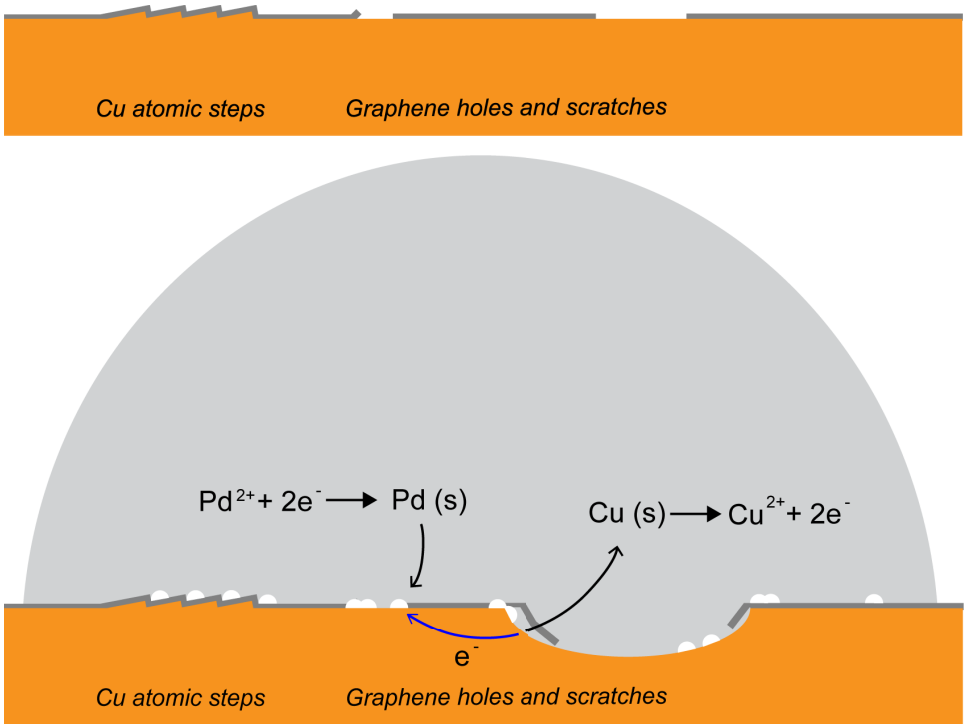

Figure 10. Proposed nanoparticle deposition mechanism via galvanic displacement through graphene. Unreacted graphene on copper, exhibiting atomic steps and hole-type defects (top); proposed nanoparticle deposition mechanism for limited contact reaction, with etch pits keeping the deposition solution in contact with the copper (bottom).

In the limited contact regime explored in this study, copper is exposed to the deposition solution only through hole-type graphene defects. Copper begins to oxidize from random defects where the copper is exposed to the solution, with electrons flowing through the copper and graphene to support palladium nucleation and growth elsewhere. This nanoparticle deposition preferentially occurs at features where surface energies are favorable, specifically copper atomic steps and other graphene holes, but also takes place at areas of the graphene/copper that are featureless to the resolution of scanning electron microscopy (molecular-scale features such as graphene point defects may be present).

As the reaction proceeds, it is aggressive enough to form etch pits in the copper, damaging the graphene layer and therefore keeping the deposition solution in contact with the copper substrate to support the continued reaction. Some nanoparticles form at and near the etch pits

themselves, but not sufficiently to seal them from further growth. Therefore, the reaction does not limit nanoparticle deposition to hole-type defects, and defect sealing is not effectively achieved. That is, the galvanic displacement reaction is not self-limiting, at least under the various conditions studied here.

During treatment with O_2 plasma, the graphene is decorated with oxygen-containing functional groups, and the copper substrate is oxidized in conjunction with graphene damage[93]. During galvanic displacement, it is possible that the palladium preferentially deposits at these functionalized regions, rather than at other features such as copper atomic steps, due to their chemical reactivity (see Figure 11). The lack of etch pits in these samples is not fully explained; perhaps the graphene is damaged by the plasma to the degree that the deposition solution's access to the copper is not limited enough to lead to etch pit formation. Another experimental observation that has not been satisfactorially rationalized is the palladium deposition morphology when the galvanic displacement reaction is conducted after FIB milling, with halos of little to no palladium deposition surrounding the sites where the graphene on copper had been bombarded with gallium ions.

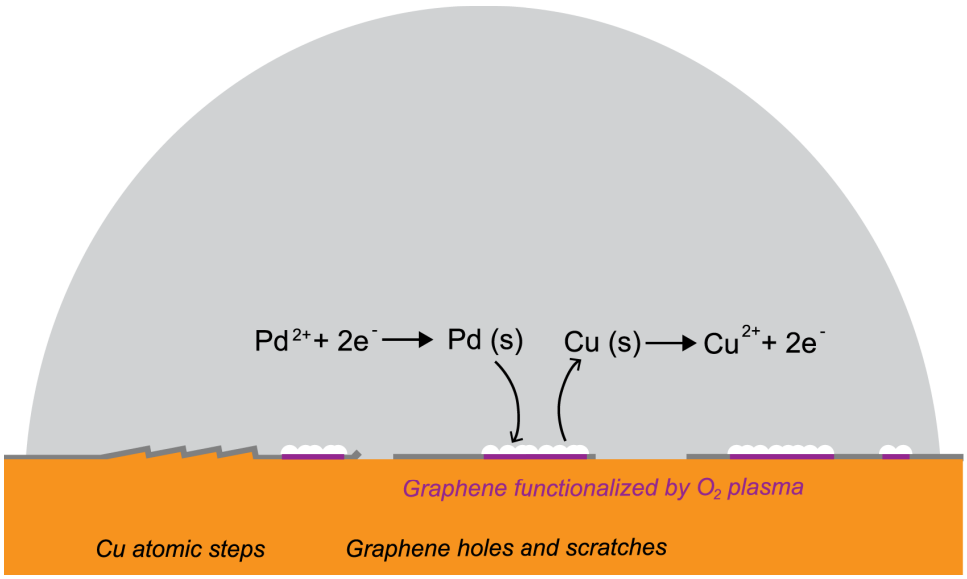

Figure 11. Possible nanoparticle deposition mechanism via galvanic displacement through graphene after O_2 plasma treatment. The palladium may preferentially deposit at portions of

the graphene functionalized/damaged by the plasma treatment, and copper etch pits are not observed.

In any case, under typical reaction conditions and in accordance with the thermodynamics of the electrochemical reaction and with classical nucleation theory, the free energy of the electrochemical reaction modulates the particle size distribution and the kinetics of nucleation. A greater ΔG_{rxn}, in this study achieved with a higher palladium concentration in the deposition solution, leads to a smaller critical radius of nucleation, a larger range of nanoparticle sizes, and faster nucleation.

4. Engineering palladium deposition for graphene membranes

4.1. Theory

Membrane separation is an energy- and space-efficient alternative to other commonly used industrial separations methods, such as distillation and absorption[95], and has been deployed at the industrial scale for applications including water treatment, chemical processing, and dialysis[96,97]. When compared to conventional dense polymeric membranes, nanoporous atomically thin membranes—made of 2D materials with nanoscale pores, typically layered over another porous membrane for mechanical support—have the advantages of ultimate thinness and therefore minimal resistance to transport; chemical and mechanical robustness; and theoretically high selectivity if pore sizes are tightly controlled and unintended defects are minimized[96,97,98]. The presence of hole-type defects in the 2D material is therefore deleterious to membrane performance, and methods of defect sealing have been investigated in an effort to realize the impressive theoretical selectivites of nanoporous atomically thin membranes[99,100,101].

In the model system investigated in this study, the galvanic displacement reaction has some competing effects of graphene sealing (via nanoparticle deposition at defects, including hole-type defects) and defect enhancement (via micron-scale copper etch pit formation at least, and possibly smaller-scale damage as well). To assess the potential of metal deposition via galvanic displacement as a method of defect sealing for graphene membranes, the presence of hole-type defects on treated and untreated graphene was investigated with a series of diffusion tests.

A porous membrane mounted between two well-stirred chambers at known concentrations of some species, C_{feed} and C_{perm}, has a concentration gradient within each of its pores (see Figure 12). In the absence of a pressure difference across the membrane, the species in solution will therefore experience diffusive transport through the membrane pores from the feed side to the permeate side.

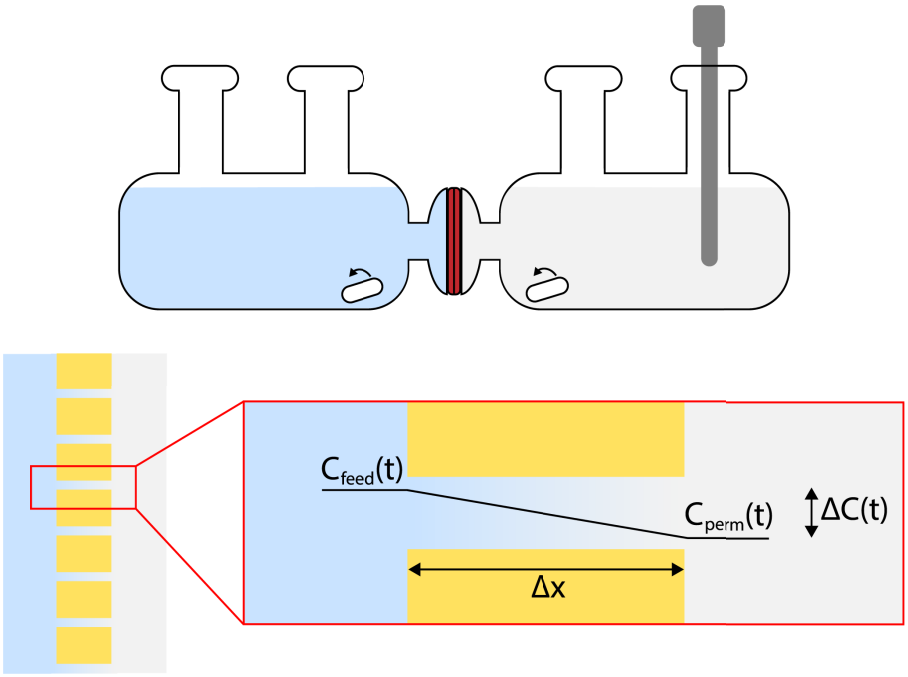

Figure 12. Diffusion test schematic: macroscale cross-sectional view of diffusion cell, with membrane mounted between feed and permeate sides and conductivity meter at the permeate side (top), and microscale cross-sectional view of a porous membrane with a concentration gradient (bottom).

Starting from Fick's First Law of Diffusion,

$$J = -D\frac{\partial \mathrm{C}}{\partial \mathrm{x}} \tag{12}$$

$$= D\frac{\Delta C(t)}{\Delta x} \tag{13}$$

where J = flux, $\left[\frac{mol}{m^2 s}\right]$

D = diffusivity, $\left[\frac{m^2}{s}\right]$

$\Delta C(t)$ = concentration difference, $C_{feed}(t) - C_{perm}(t)$

Δx = pore length, here taken as membrane thickness

If the feed and permeate sides have equal volumes and the rates of change of their concentrations are therefore equal and opposite,

$$\frac{dC_{perm}}{dt} = -\frac{dC_{feed}}{dt} = \frac{J\alpha A_{mem}A_{pore}}{V} \tag{14}$$

where α = pore number density per unit membrane area

A_{mem} = total membrane area

A_{pore} = area of one pore

V = feed side volume = permeate side volume

The membrane permeance can be defined as the mass transfer rate per unit area of membrane per unit driving force (the driving force for diffusive transport being the concentration difference),

$$P = \frac{J\alpha A_{mem}A_{pore}}{A_{mem}\Delta C(t)} \tag{15}$$

$$= \frac{D\frac{\Delta C(t)}{\Delta x}\alpha A_{mem}A_{pore}}{A_{mem}\Delta C(t)} \tag{16}$$

$$= \frac{D\alpha A_{pore}}{\Delta x} \tag{17}$$

where P = permeance, $\left[\frac{m}{s}\right]$

This expression can be rewritten in terms of quantities known or measured in diffusion cell experiments,

$$P = \frac{\frac{dC_{perm}}{dt}V}{A_{mem}\Delta C(t)} \tag{18}$$

Therefore, for a membrane for which the pore number density, pore size, and pore length are known, a theoretical permeance of a known species through the membrane can be calculated and compared with the permeance obtained from a curve fit to diffusion test data.

As pristine graphene is impermeable to even the smallest gases[102], a pristine layer of graphene layered over a nanoporous support membrane should result in zero diffusive transport through the membrane. In reality, however, graphene's intrinsic hole-type defects from the CVD growth process, as well as larger-scale defects introduced during graphene handling[103,104], mean that transport will indeed occur where hole-type defects align with the support membrane's pores (see Figure 13).

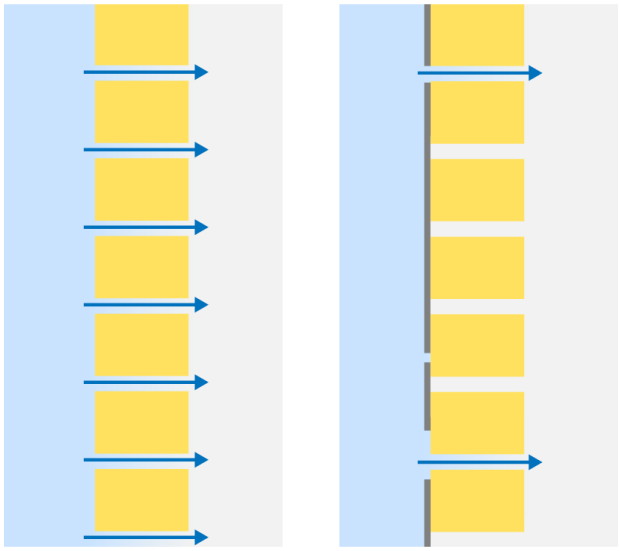

Figure 13. Cross-sectional schematic of diffusion through nanoporous membrane without (left) and with (right) a graphene layer, exhibiting diffusive transport where the graphene's hole-type defects align with the support membrane's pores.

A parameter can thus be introduced to characterize graphene-sealed membranes by comparing their permeance to the unsealed support membrane permeance,

$$C \equiv \left(1 - \frac{P}{P_{support}}\right) * 100\% \tag{19}$$

where C = coverage

$P_{support}$ = support membrane permeance, $\left[\frac{m}{s}\right]$

4.2. Nanoparticle survival

In the few existing studies investigating galvanic displacement between ions in solution and copper foil across single-layer graphene, researchers used polymer-assisted and/or direct transfer methods to remove the decorated graphene from the copper substrate and transfer it to SiO_2/Si for imaging and Si, PET, and glass for use in devices[53,54,55]. Images as well as device performance data indicate that the deposited nanostructures remain on the graphene surface after these transfer processes[53,54,55], suggesting that the nanoparticles' attachment to the graphene substrate is not too fragile for use of the decorated graphene in device applications.

In the context of these established results, the purpose of explicitly confirming nanoparticle survival upon transfer to a nanoporous polyimide support membrane in this study is twofold. Firstly, only a few studies of this type of system exist, and it is useful to confirm the robustness of this nanofabrication method to a different lab's graphene transfer protocol and to a different type of support than previously studied. Secondly, for practical use of the nanoparticle-decorated graphene as a membrane material, it is important to establish whether nanoparticles remain attached to the graphene not just during the process of transferring the graphene to a support membrane but also during mounting in a diffusion cell and use as a membrane.

After depositing palladium nanoparticles onto a graphene/copper surface via submersion in the deposition solution, the palladium-decorated graphene was transferred to a polyimide support membrane with 20 nanometer pores (PI 20 nm) and the resulting membrane was tested in a diffusion cell. The membrane was then allowed to fully dry and observed with SEM imaging. Graphene transfer, diffusion test, and SEM methods are described in detail in Section 2.

SEM imaging clearly shows that many palladium nanoparticles survive the polymer-assisted transfer process and the diffusion test (see Figure 14). Analysis by hand of SEM images of palladium nanoparticles on graphene/copper without transfer to a support membrane showed approximately 170 nanoparticles per μm^2, between 8 and 119 nm in diameter (see Figure 7), while analysis of the transferred sample showed 104 nanoparticles per μm^2, the smallest nanoparticle being 7 nm and the largest being 109 nm in diameter. While the counted nanoparticle number density is lower in the transferred sample, the size range is similar, indicating that nanoparticles towards both the smaller and larger ends of the size distribution survived.

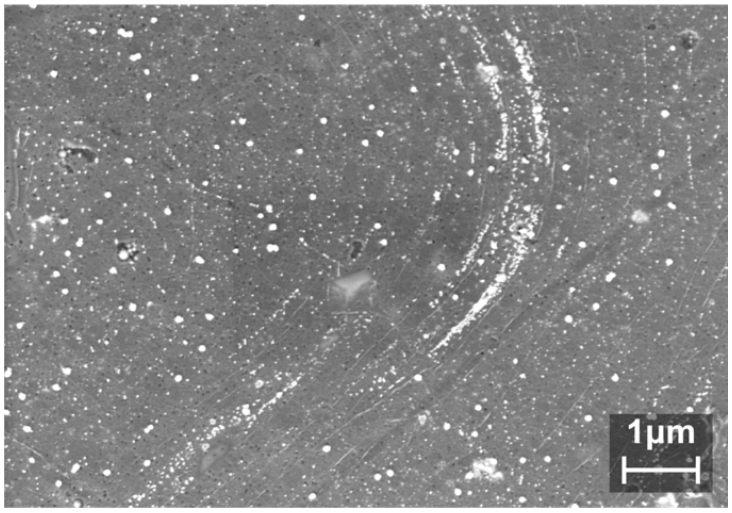

Figure 14. Palladium nanoparticles on graphene on PI 20 nm, after a diffusion test. Nanoparticles' alignment with where the copper atomic steps had been can be observed. The dark, very small dots are the support membrane's pores. The region shown in this image did not come into contact with the silicone gaskets. Submerged in 0.1 mM $PdCl_2$ + 3 mM NaCl, 5 min reaction time, transferred to PI 20 nm.

It should be noted that it is more challenging to image graphene once it is transferred to a polyimide substrate due to polyimide being nonconductive, which led to discrepancies in image quality that may have affected the nanoparticle counting and size range determination processes. Furthermore, in the absence of automated image processing methods, SEM analysis

was done by hand on 1 μm^2 sections of the images, which does not fully take into account spatial heterogeneity in deposition.

Many nanoparticles in the transferred sample can be observed to follow curved lines, indicating that the deposited morphology along the atomic steps of the copper substrate was preserved. Furthermore, many nanoparticles – as well as much of the underlying graphene, although some bare patches were observed – unexpectedly survived in the region of the graphene that had been pressed between two silicone gaskets for diffusion cell mounting.

These results demonstrate some degree of robustness of the nanoparticles to graphene handling after deposition. Not only did many small and large nanoparticles survive the transfer process, they remained after the diffusion test, including the mounting and removal processes. While the approximate nanoparticle number density was lower on the transferred sample than the untransferred sample, indicating that some nanoparticles may have been dislodged, the exact degree of particle dislodgement could not be determined conclusively due to difficulties in the imaging and nanoparticle counting processes. Further study using more robust image analysis methods may therefore be warranted.

4.3. Defect sealing

Potassium chloride diffusion tests were conducted for a bare PI 20 nm membrane, graphene on PI 20 nm, and graphene decorated with palladium nanoparticles via submersion in the deposition solution and subsuquently transferred to PI 20 nm. Three separate centimeter-scale membranes were synthesized and tested for each of these three membrane types, for a total of nine membranes. All graphene was from the same batch to eliminate the effects of discrepancies in graphene quality between batches. Conductivity time series data collected at the permeate side during the diffusion test were converted to KCl concentration, and the resulting curves were fit with Equation 18 to obtain permeance values (see Figure 15). See

Section 2 for more details of the graphene transfer and diffusion test experimental procedures.

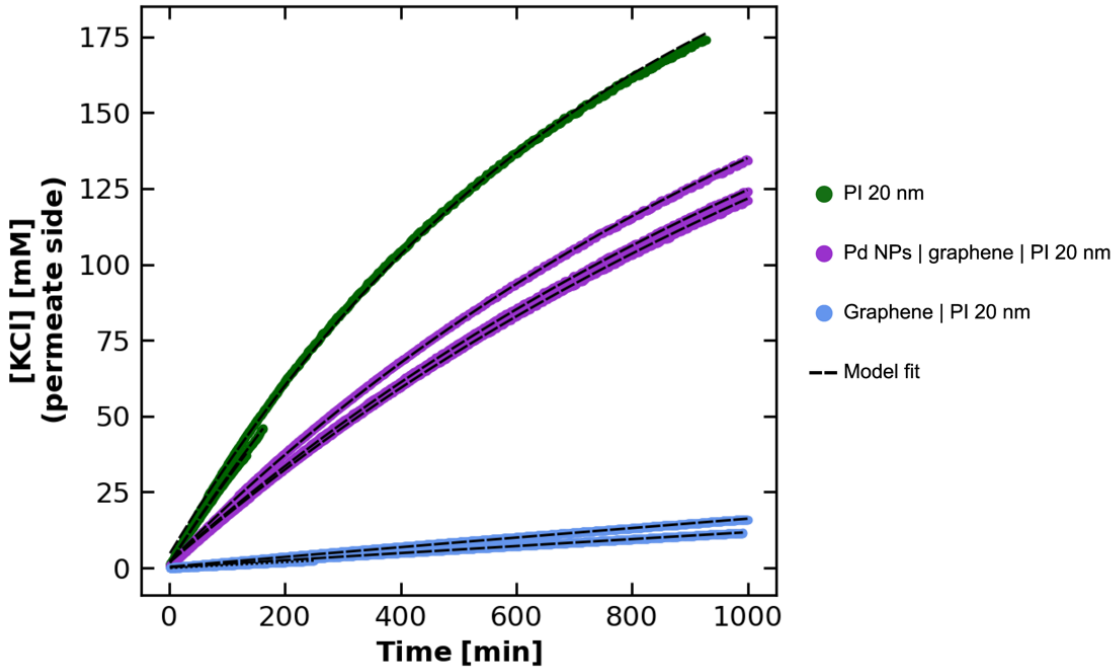

Figure 15. Permeate side potassium chloride concentration vs. time during diffusion testing of bare PI 20 nm, nanoparticle-decorated graphene on PI 20 nm, and unreacted graphene on PI 20 nm. Three separate membranes were synthesized and tested under the same conditions for each type of membrane, for a total of nine membranes. Curves were fit to Equation 18 to obtain permeance values (with the exception of one curve, which was fit to a linearized version that yielded a better fit); greater slope corresponds to higher permeance. Decorated graphene was submerged in 0.1 mM $PdCl_2$ + 3 mM NaCl, 5 min reaction time, and transferred to PI 20 nm.

The bare PI 20 nm membrane's measured permeance, 2.454 x 10^{-6} m/s, was in the same order of magnitude as the theoretical value predicted using Equation 17, 4.345 x 10^{-6} m/s (using potassium chloride diffusivity as measured by He et al.[105]), indicating that the diffusion experiments were conducted correctly. The unreacted graphene on PI 20 nm had the lowest permeance (1.019 x 10^{-7} m/s) and highest coverage (95.8%), with the nanoparticle-decorated

graphene's permeance (1.404 x 10^{-6} m/s) and coverage (42.8%) reflecting a much higher degree of leakage (see Figure 16).

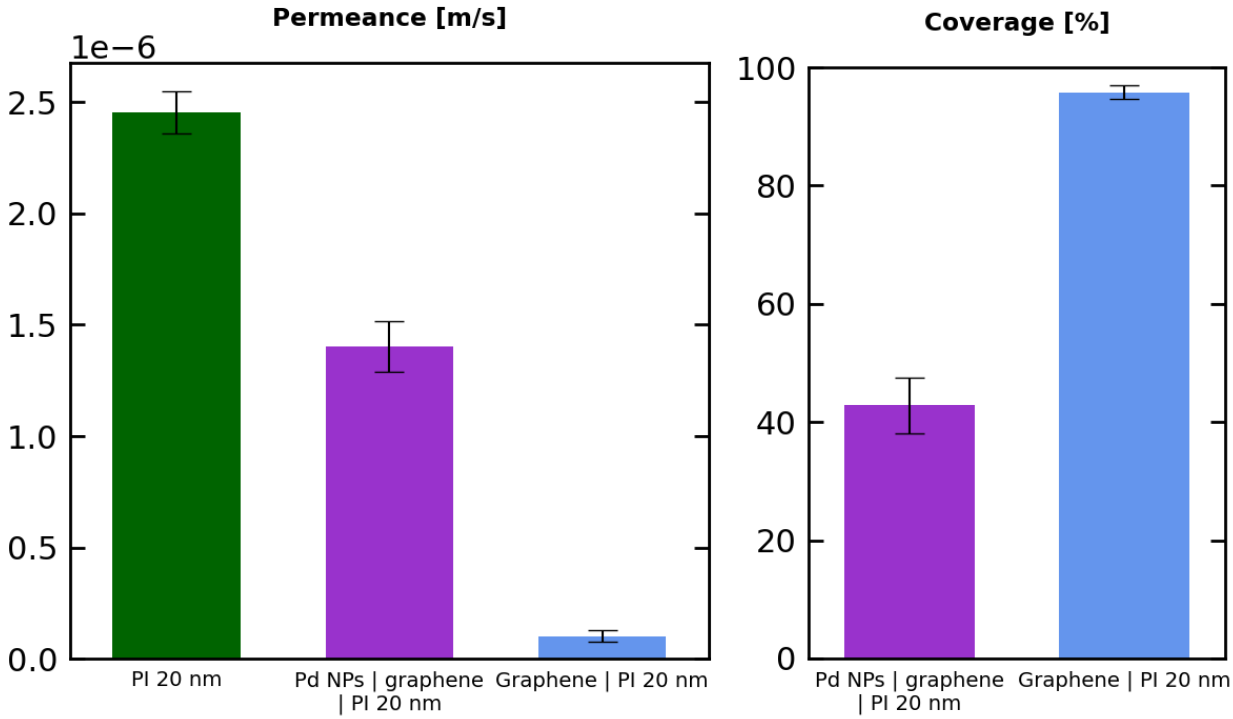

Figure 16. Membrane permeance and coverage for bare PI 20 nm, nanoparticle-decorated graphene on PI 20 nm, and unreacted graphene on PI 20 nm. Error bars show one standard deviation. Decorated graphene was submerged in 0.1 mM $PdCl_2$ + 3 mM NaCl, 5 min reaction time, and transferred to PI 20 nm.

These results indicate that the galvanic displacement reaction has a net effect of enhancing rather than sealing hole-type defects in the graphene. Therefore, under the reaction conditions tested here, galvanic displacement was unsuccessful as a method to seal defects for the preparation of graphene membranes. However, many nanoparticles did survive the transfer, mounting, and diffusion testing processes, as described in Section 4.2, indicating that defect sealing may in fact be achieveable using this method. Future sudy should focus on careful engineering of the galvanic displacement reaction conditions to control the presence and size of etch pits, as well as developing advanced image processing methods to confirm the exact degree of nanoparticle survival.

5. Conclusion

5.1. Summary of findings

2D materials modified or functionalized with nanostructures have shown promise in diverse applications, from medicine to catalysis to energy and beyond[2,3,4,5,6,7]. Despite inherent challenges in achieving tight control over the deposition process, galvanic displacement has garnered research interest as a facile, versatile, and quick method of depositing a wide array of metal nanostructures[17,18,19,20,21,22,23,24,25,26,27,28], but has not been deeply explored as a method of depositing nanostructures on 2D materials in particular. Building upon the work of Hong et al., depositing palladium nanoparticles on graphene via galvanic displacement between a palladium ion deposition solution and the graphene's copper substrate[54,55], this thesis examines two questions: How can palladium deposition in this system be controlled, and can this nanofabrication technique be exploited to seal graphene holes for the synthesis of nanoporous atomically thin membranes?

First, the effects of limited solution-copper contact, varied palladium concentration, and O_2 plasma and FIB surface pre-treatments were investigated. In accordance with the predictions of basic electrochemical thermodynamics and classical nucleation theory, the thermodynamic driving force of the galvanic displacement reaction, here modulated via the deposition solution's palladium (II) concentration, determines the nanoparticle size range and speed of nucleation, with a higher palladium concentration leading to faster nucleation and a smaller critical radius for nanoparticle survival.

Under the conditions tested, micron-scale copper etch pits are found to play a critical role in the behavior of the reaction. These etch pits maintain contact between the deposition solution and the copper substrate and thus lead to non-self-limited palladium deposition. In conjunction with graphene's high electrical conductivity, this causes preferential deposition not only at holes where the copper is directly exposed to the deposition solution but also at non-hole-type features where surface energies are presumably favorable for nucleation, namely atomic steps

in the copper substrate. The observation of copper etch pits after galvanic displacement parallels findings from studies of graphene as a corrosion mitigation material. While graphene with zero hole-type defects would theoretically isolate its substrate from the environment and thus totally prevent corrosion, graphene's electrically conductive (and often cathodic) nature exacerbates localized corrosion at holes in the graphene layer[36,45,46,47,48].

Galvanic displacement was finally investigated as a possible method of sealing graphene defects for the creation of nanoporous atomically thin membranes. Centimeter-scale membranes fabricated with graphene that had been treated via galvanic displacement experience increased leakage, likely due to graphene damage at the etch pits inherent to this deposition mechanism. However, membrane imaging did reveal that many palladium nanoparticles survive polymer-assisted graphene transfer from the copper foil to the porous support membrane, as well as mounting and use in diffusion testing. If the issue of copper etch pits were resolved, graphene sealing via the deposition of nanoparticles by galvanic displacement may therefore be possible, since many nanoparticles do not detach from the graphene during these processes.

5.2. Future directions

For future study of this system, a kinetic treatment of palladium nucleation, perhaps in conjunction with measurement of the electrical potential at the graphene/copper surface during the reaction, would further elucidate the details of palladium deposition. It may also be illuminating to further explore the non-contact-limited regime by fully removing graphene from one side of the copper foil. This may replicate the preferential deposition patterns observed by Hong et al. that were not observed in this study, such as deposition at graphene wrinkles and grain boundaries[55]. Automated image processing methods, while not achieved in this study due to background features that made thresholding extremely challenging, would be very useful for analyzing SEM images in a consistent manner and extracting complete nanoparticle size distributions rather than just approximate size ranges and number densities.

To tip the effect of galvanic displacement from net defect enhancement to defect sealing for membrane applications, galvanic displacement under less-aggressive conditions (i.e. lower deposition solution palladium concentration) may help address the copper etch pit issue, as etch pits were observed to be smallest after deposition with the lowest palladium concentration used in this study. A non-contact-limited regime, with a larger area of copper exposed to the deposition solution, may also help to address this.

Hong et al. fabricated a hydrogen gas sensor[54] and transparent, flexible heater[55] using graphene decorated with palladium via galvanic displacement, in addition to the nanoporous atomically thin membrane application explored here. Many other possible applications of this nanofabrication technique are open for exploration and development. Depending upon the intended functionality, the principles explored in this study may be adapted to easily deposit non-palladium noble metals on single-layer graphene via galvanic displacement with the copper substrate (e.g. silver nanoparticles for antimicrobial effects[2]), as demonstrated by silver and gold deposition using this method in previous studies[53,55].

Finally, galvanic displacement through 2D materials other than graphene is an interesting area for further exploration. In particular, nonconductive 2D materials, such as hexagonal boron nitride or molybdenum disulfide, may lead to a higher degree of control over deposition. In these cases, nucleation may be limited to hole-type defects, as there would be no route for electron flow to support deposition at other features of the surface.

While galvanic displacement is challenging to control, as demonstrated by the etch pits damaging graphene in this study, its efficacy in decorating graphene with palladium nanoparticles has clearly been demonstrated, along with some knobs available to tune this process. With further development, galvanic displacement may become a robust nanofabrication tool to modify not only graphene but also other 2D materials, helping to unlock the combined potential of 2D materials and nanostructures to engineer technologies relevant to a healthy, sustainable future.

Bibliography

1. Novoselov, K. S. *et al.* Electric Field Effect in Atomically Thin Carbon Films. *Science* **306**, 666–669 (2004).
2. Kurapati, R., Kostarelos, K., Prato, M. & Bianco, A. Biomedical Uses for 2D Materials Beyond Graphene: Current Advances and Challenges Ahead. *Adv. Mater.* **28**, 6052–6074 (2016).
3. Lee, C. W., Suh, J. M. & Jang, H. W. Chemical Sensors Based on Two-Dimensional (2D) Materials for Selective Detection of Ions and Molecules in Liquid. *Frontiers in Chemistry* **7**, (2019).
4. Koyappayil, A., Yagati, A. K. & Lee, M.-H. Recent Trends in Metal Nanoparticles Decorated 2D Materials for Electrochemical Biomarker Detection. *Biosensors* **13**, 91 (2023).
5. Li, T. *et al.* The Combination of Two-Dimensional Nanomaterials with Metal Oxide Nanoparticles for Gas Sensors: A Review. *Nanomaterials* **12**, 982 (2022).
6. Deng, J., Deng, D. & Bao, X. Robust Catalysis on 2D Materials Encapsulating Metals: Concept, Application, and Perspective. *Adv. Mater.* **29**, 1606967 (2017).
7. Jeong, G. H. *et al.* Nanoscale Assembly of 2D Materials for Energy and Environmental Applications. *Adv. Mater.* **32**, 1907006 (2020).
8. Cookson, J. The Preparation of Palladium Nanoparticles. *platin met rev* **56**, 83–98 (2012).
9. Chen, A. & Ostrom, C. Palladium-Based Nanomaterials: Synthesis and Electrochemical Applications. *Chem. Rev.* **115**, 11999–12044 (2015).
10. Novoselov, K. S. *et al.* A roadmap for graphene. *Nature* **490**, 192–200 (2012).
11. Volta, A. On the electricity excited by the mere contact of conducting substances of different kinds. *Philosophical Transactions of the Royal Society of London* **90**, 403–431 (1800).
12. *Electrochemistry, Past and Present*. vol. 390 (American Chemical Society, 1989).
13. Luigi Galvani. *ETHW* https://ethw.org/Luigi_Galvani (2016).
14. Koch, G. 1 - Cost of corrosion. in *Trends in Oil and Gas Corrosion Research and Technologies* (ed. El-Sherik, A. M.) 3–30 (Woodhead Publishing, 2017).
15. Shaw, B. & Kelly, R. What is Corrosion? *Electrochem. Soc. Interface* **15**, 24 (2006).
16. Kaesche, H. *Corrosion of Metals: Physicochemical Principles and Current Problems*. (Springer Science & Business Media, 2003).
17. Carraro, C., Maboudian, R. & Magagnin, L. Metallization and nanostructuring of semiconductor surfaces by galvanic displacement processes. *Surface Science Reports* **62**, 499–525 (2007).

18. Baek, S., Kim, K. H., Kim, M. J. & Kim, J. J. Morphology control of noble metal catalysts from planar to dendritic shapes by galvanic displacement. *Applied Catalysis B: Environmental* **217**, 313–321 (2017).

19. Gutés, A., Carraro, C. & Maboudian, R. Ultrasmooth Gold Thin Films by Self-Limiting Galvanic Displacement on Silicon. *ACS Appl. Mater. Interfaces* **3**, 1581–1584 (2011).

20. Zhang, Y., Diao, W., Monnier, J. R. & Williams, C. T. Pd–Ag/SiO_2 bimetallic catalysts prepared by galvanic displacement for selective hydrogenation of acetylene in excess ethylene. *Catal. Sci. Technol.* **5**, 4123–4132 (2015).

21. Tang, L. *et al.* Glucose sensor based on Pd nanosheets deposited on Cu/Cu2O nanocomposites by galvanic replacement. *Colloids and Surfaces B: Biointerfaces* **188**, 110797 (2020).

22. Tran, M. *et al.* Formation of Size and Density Controlled Nanostructures by Galvanic Displacement. *Nanomaterials* **10**, 644 (2020).

23. Sayed, S. Y. & Buriak, J. M. Epitaxial Growth of Nanostructured Gold Films on Germanium via Galvanic Displacement. *ACS Appl. Mater. Interfaces* **2**, 3515–3524 (2010).

24. Vasilic, R. & Dimitrov, N. Epitaxial Growth by Monolayer-Restricted Galvanic Displacement. *Electrochem. Solid-State Lett.* **8**, C173 (2005).

25. Liu, R., Sha, T., Zhou, Q. & Nie, B. Copper-surrogated galvanic displacement of silver dendrite imprinted on flexible and transparent silk fibroin membrane as a SERS-active substrate and sub-dividable catalyst. *Applied Surface Science* **470**, 1003–1009 (2019).

26. Biemolt, J. *et al.* Assembling Palladium and Cuprous Oxide Nanoclusters into Single Quantum Dots for the Electrocatalytic Oxidation of Formaldehyde, Ethanol, and Glucose. *ACS Appl. Nano Mater.* **3**, 10176–10182 (2020).

27. Ali, H. O. & Christie, I. R. A. A review of electroless gold deposition processes. *Gold Bull.* **17**, 118–127 (1984).

28. Liu, R. & Sen, A. Unified Synthetic Approach to Silver Nanostructures by Galvanic Displacement Reaction on Copper: From Nanobelts to Nanoshells. *Chem. Mater.* **24**, 48–54 (2012).

29. Alia, S. M., Yan, Y. S. & Pivovar, B. S. Galvanic displacement as a route to highly active and durable extended surface electrocatalysts. *Catal. Sci. Technol.* **4**, 3589–3600 (2014).

30. Magagnin, L., Maboudian, R. & Carraro, C. Gold Deposition by Galvanic Displacement on Semiconductor Surfaces: Effect of Substrate on Adhesion. *J. Phys. Chem. B* **106**, 401–407 (2002).

31. Shi, M. *et al.* 2D/2D-Ni–Co–B/rGO Nanolayers Prepared by Galvanic Replacement for Hydrogen Generation through NaBH4 Hydrolysis. *ACS Appl. Nano Mater.* **6**, 6798–6809 (2023).

32. Alfi, N., Yazdan-Abad, M. Z., Rezvani, A., Noroozifar, M. & Khorasani-Motlagh, M. Three-dimensional Pd-Cd nanonetwork decorated on reduced graphene oxide by a galvanic

method as a novel electrocatalyst for ethanol oxidation in alkaline media. *Journal of Power Sources* **396**, 742–748 (2018).

33. Brankovic, S. R., Wang, J. X. & Adžić, R. R. Metal monolayer deposition by replacement of metal adlayers on electrode surfaces. *Surface Science* **474**, L173–L179 (2001).
34. Dryfe, R. A. W., Walter, E. C. & Penner, R. M. Electrodeposition of Metal Nanostructures by Galvanic Displacement Powered with Insoluble Crystals of a Ferrocene Derivative. *ChemPhysChem* **5**, 1879–1884 (2004).
35. daRosa, C. P., Iglesia, E. & Maboudian, R. Dynamics of Copper Deposition onto Silicon by Galvanic Displacement. *J. Electrochem. Soc.* **155**, D244 (2008).
36. Tanjil, M. R.-E., Jeong, Y., Yin, Z., Panaccione, W. & Wang, M. C. Ångström-Scale, Atomically Thin 2D Materials for Corrosion Mitigation and Passivation. *Coatings* **9**, 133 (2019).
37. Chen, S. *et al.* Oxidation Resistance of Graphene-Coated Cu and Cu/Ni Alloy. *ACS Nano* **5**, 1321–1327 (2011).
38. Kirkland, N. T., Schiller, T., Medhekar, N. & Birbilis, N. Exploring graphene as a corrosion protection barrier. *Corrosion Science* **56**, 1–4 (2012).
39. Nilsson, L. *et al.* Graphene Coatings: Probing the Limits of the One Atom Thick Protection Layer. *ACS Nano* **6**, 10258–10266 (2012).
40. Prasai, D., Tuberquia, J. C., Harl, R. R., Jennings, G. K. & Bolotin, K. I. Graphene: Corrosion-Inhibiting Coating. *ACS Nano* **6**, 1102–1108 (2012).
41. Nayak, P. K., Hsu, C.-J., Wang, S.-C., Sung, J. C. & Huang, J.-L. Graphene coated Ni films: A protective coating. *Thin Solid Films* **529**, 312–316 (2013).
42. Mišković-Stanković, V., Jevremović, I., Jung, I. & Rhee, K. Electrochemical study of corrosion behavior of graphene coatings on copper and aluminum in a chloride solution. *Carbon* **75**, 335–344 (2014).
43. Ahn, Y., Jeong, Y. & Lee, Y. Improved Thermal Oxidation Stability of Solution-Processable Silver Nanowire Transparent Electrode by Reduced Graphene Oxide. *ACS Appl. Mater. Interfaces* **4**, 6410–6414 (2012).
44. Kang, D. *et al.* Oxidation Resistance of Iron and Copper Foils Coated with Reduced Graphene Oxide Multilayers. *ACS Nano* **6**, 7763–7769 (2012).
45. Sai Pavan, A. S. & Ramanan, S. R. A study on corrosion resistant graphene films on low alloy steel. *Appl Nanosci* **6**, 1175–1181 (2016).
46. Zhou, F., Li, Z., Shenoy, G. J., Li, L. & Liu, H. Enhanced Room-Temperature Corrosion of Copper in the Presence of Graphene. *ACS Nano* **7**, 6939–6947 (2013).
47. Cui, C., Lim, A. T. O. & Huang, J. A cautionary note on graphene anti-corrosion coatings. *Nature Nanotech* **12**, 834–835 (2017).

48. Xu, Y., Qu, J., Shen, Y. & Feng, W. Different graphene layers to enhance or prevent corrosion of polycrystalline copper. *RSC Advances* **8**, 15181–15187 (2018).

49. Cui, C., Lim, A. T. O. & Huang, J. A cautionary note on graphene anti-corrosion coatings. *Nature Nanotech* **12**, 834–835 (2017).

50. Mujib, S. B., Mukherjee, S., Ren, Z. & Singh, G. Assessing corrosion resistance of two-dimensional nanomaterial-based coatings on stainless steel substrates. *Royal Society Open Science* **7**, 200214 (2020).

51. Song, B. *et al.* In situ study of nucleation and growth dynamics of Au nanoparticles on MoS2 nanoflakes. *Nanoscale* **10**, 15809–15818 (2018).

52. Shi, M. *et al.* 2D/2D-Ni–Co–B/rGO Nanolayers Prepared by Galvanic Replacement for Hydrogen Generation through NaBH4 Hydrolysis. *ACS Appl. Nano Mater.* **6**, 6798–6809 (2023).

53. Ho, P. *et al.* Self-Crack-Filled Graphene Films by Metallic Nanoparticles for High-Performance Graphene Heterojunction Solar Cells. *Advanced Materials* **27**, 1724–1729 (2015).

54. Hong, J. *et al.* A Highly Sensitive Hydrogen Sensor with Gas Selectivity Using a PMMA Membrane-Coated Pd Nanoparticle/Single-Layer Graphene Hybrid. *ACS Appl. Mater. Interfaces* **7**, 3554–3561 (2015).

55. Hong, J. *et al.* A Facile Method for Selective Decoration of Graphene Defects Based on a Galvanic Displacement Reaction. *NPG Asia Materials* **8**, (2016).

56. Ji, H., Li, M., Wang, Y. & Gao, F. Electrodeposition of graphene-supported PdPt nanoparticles with enhanced electrocatalytic activity. *Electrochemistry Communications* **24**, 17–20 (2012).

57. Yang, S. *et al.* One-Pot Synthesis of Graphene-Supported Monodisperse Pd Nanoparticles as Catalyst for Formic Acid Electro-oxidation. *Sci Rep* **4**, 4501 (2014).

58. Kakaei, K. & Dorraji, M. One-pot synthesis of Palladium Silver nanoparticles decorated reduced graphene oxide and their application for ethanol oxidation in alkaline media. *Electrochimica Acta* **143**, 207–215 (2014).

59. Lv, J.-J. *et al.* One-pot synthesis of monodisperse palladium–copper nanocrystals supported on reduced graphene oxide nanosheets with improved catalytic activity and methanol tolerance for oxygen reduction reaction. *Journal of Power Sources* **269**, 104–110 (2014).

60. Khan, M. *et al.* Facile synthesis of Pd@graphene nanocomposites with enhanced catalytic activity towards Suzuki coupling reaction. *Sci Rep* **10**, 11728 (2020).

61. Chen, C.-H. *et al.* Hydrogen storage performance in palladium-doped graphene/carbon composites. *International Journal of Hydrogen Energy* **38**, 3681–3688 (2013).

62. Lu, L.-M. *et al.* In situ synthesis of palladium nanoparticle–graphene nanohybrids and their application in nonenzymatic glucose biosensors. *Biosensors and Bioelectronics* **26**, 3500–3504 (2011).

63. Zeng, Q., Cheng, J.-S., Liu, X.-F., Bai, H.-T. & Jiang, J.-H. Palladium nanoparticle/chitosan-grafted graphene nanocomposites for construction of a glucose biosensor. *Biosensors and Bioelectronics* **26**, 3456–3463 (2011).

64. Ye, R. & Tour, J. M. Graphene at Fifteen. *ACS Nano* **13**, 10872–10878 (2019).

65. Buy Graphene Films Processed in Clean Room Class 1000. *Graphenea* https://www.graphenea.com/collections/buy-graphene-films.

66. Polycarbonate Track-etched membrane filters | It4ip | ipPORE™. *it4ip* https://www.it4ip-iontracktechnology.com/product-portfolio/ippore/.

67. Direct-Q® 3 UV Water Purification System | ZRQSVP3WW. https://www.emdmillipore.com/US/en/product/Direct-Q-3-UV-Water-Purification-System,MM_NF-ZRQSVP3WW.

68. Adobe Illustrator. https://www.adobe.com/products/illustrator.html.

69. OpenCV: OpenCV modules. https://docs.opencv.org/4.x/.

70. The Python Language Reference. *Python documentation* https://docs.python.org/3/reference/index.html.

71. Expanded Plasma Cleaner. *Harrick Plasma* https://harrickplasma.com/plasma-cleaners/expanded-plasma-cleaner/.

72. Side-Bi-Side Cells. *PermeGear* https://permegear.com/side-bi-side-cells/.

73. SevenCompact Cond meter S230. *Mettler Toledo* https://www.mt.com/us/en/home/phased_out_products/Laboratory_Analytics_Browse/pH-meter/pH-meters/benchtop-pH-meter/sevencompact/S230-Meter.html.

74. Vanysek, P. Electrochemical Series.

75. Tsuji, J. *Organic Synthesis with Palladium Compounds*. vol. 10 (Springer Berlin Heidelberg, 1980).

76. Tait, C. D., Janecky, D. R. & Rogers, P. Z. Speciation of aqueous palladium(I1) chloride solutions using optical spectroscopies. *Geochimica et Cosmochimica Acta* **55**, 1253–1264 (1991).

77. Cruywagen, J. J. & Kriek, R. J. Complexation of palladium(II) with chloride and hydroxide. *Journal of Coordination Chemistry* **60**, 439–447 (2007).

78. Wang, Y., Wang, S., Chang, H. & Rao, W. Galvanic Replacement of Liquid Metal/Reduced Graphene Oxide Frameworks. *Advanced Materials Interfaces* **7**, 2000626 (2020).

79. Volmer, M. & Weber, A. Z. Nucleus Formation in Supersaturated Systems. *Phys. Chem.* **119**, 277—301 (1926).

80. Becker, R. & Döring, W. Kinetic treatment of the nucleation in supersaturated vapors. *Annalen der Physik* **5**, (1935).

81. Oxtoby, D. W. Homogeneous nucleation: theory and experiment. *J. Phys.: Condens. Matter* **4**, 7627–7650 (1992).

82. Davies, S. Nucleation Theory: A Literature Review and Applications to Nucleation Rates of Natural Gas Hydrates.

83. Hu, Q. *et al.* The thermodynamics of calcite nucleation at organic interfaces: Classical vs. non-classical pathways. *Faraday Discuss.* **159**, 509–523 (2013).

84. Jun, Y.-S., Kim, D. & Neil, C. W. Heterogeneous Nucleation and Growth of Nanoparticles at Environmental Interfaces. *Acc. Chem. Res.* **49**, 1681–1690 (2016).

85. De Yoreo, J. J., Waychunas, G. A., Jun, Y.-S. & Fernandez-Martinez, A. In situ Investigations of Carbonate Nucleation on Mineral and Organic Surfaces. *Reviews in Mineralogy and Geochemistry* **77**, 229–257 (2013).

86. Oxtoby, D. W. Nucleation of First-Order Phase Transitions. *Acc. Chem. Res.* **31**, 91–97 (1998).

87. Cassar, D. R. Solving the Classical Nucleation Theory with respect to the surface energy. *Journal of Non-Crystalline Solids* **511**, 183–185 (2019).

88. Karthika, S., Radhakrishnan, T. K. & Kalaichelvi, P. A Review of Classical and Nonclassical Nucleation Theories. *Crystal Growth & Design* **16**, 6663–6681 (2016).

89. Jun, Y.-S. *et al.* Classical and Nonclassical Nucleation and Growth Mechanisms for Nanoparticle Formation. *Annu. Rev. Phys. Chem.* **73**, 453–477 (2022).

90. Fan, L. *et al.* Step driven competitive epitaxial and self-limited growth of graphene on copper surface. *AIP Advances* **1**, 032145 (2011).

91. Lisi, N. *et al.* Contamination-free graphene by chemical vapor deposition in quartz furnaces. *Sci Rep* **7**, 9927 (2017).

92. Scale-Up of CVD graphene on Cu Foil | CVD Equipment Corp. https://cvdmaterialscorporation.com/2014/05/09/low-cost-high-volume-scale-up-of-cvd-graphene-on-cu-foil/.

93. Hui, L. S., Whiteway, E., Hilke, M. & Turak, A. Synergistic oxidation of CVD graphene on Cu by oxygen plasma etching. *Carbon* **125**, 500–508 (2017).

94. Hui, L. S., Whiteway, E., Hilke, M. & Turak, A. Effect of post-annealing on the plasma etching of graphene-coated-copper. *Faraday Discuss.* **173**, 79–93 (2014).

95. Gin, D. L. & Noble, R. D. Designing the Next Generation of Chemical Separation Membranes. *Science* **332**, 674–676 (2011).

96. Wang, L. *et al.* Fundamental transport mechanisms, fabrication and potential applications of nanoporous atomically thin membranes. *Nature Nanotech* **12**, 509–522 (2017).

97. Prozorovska, L. & Kidambi, P. R. State-of-the-Art and Future Prospects for Atomically Thin Membranes from 2D Materials. *Advanced Materials* **30**, 1801179 (2018).

98. Zheng, Z., Grünker, R. & Feng, X. Synthetic Two-Dimensional Materials: A New Paradigm of Membranes for Ultimate Separation. *Adv. Mater.* **28**, 6529–6545 (2016).

99. Cheng, P. *et al.* Facile Size-Selective Defect Sealing in Large-Area Atomically Thin Graphene Membranes for Sub-Nanometer Scale Separations. *Nano Lett.* **20**, 5951–5959 (2020).

100. Jang, D., Bakli, C., Chakraborty, S. & Karnik, R. Molecular Self-Assembly Enables Tuning of Nanopores in Atomically Thin Graphene Membranes for Highly Selective Transport. *Advanced Materials* **34**, 2108940 (2022).

101. O'Hern, S. C. *et al.* Nanofiltration across Defect-Sealed Nanoporous Monolayer Graphene. *Nano Lett.* **15**, 3254–3260 (2015).

102. Bunch, J. S. *et al.* Impermeable Atomic Membranes from Graphene Sheets. *Nano Lett.* **8**, 2458–2462 (2008).

103. Boutilier, M. S. H. *et al.* Molecular Sieving Across Centimeter-Scale Single-Layer Nanoporous Graphene Membranes. *ACS Nano* **11**, 5726–5736 (2017).

104. O'Hern, S. C. *et al.* Selective Molecular Transport through Intrinsic Defects in a Single Layer of CVD Graphene. *ACS Nano* **6**, 10130–10138 (2012).

105. He, M. G., Zhang, S., Zhang, Y. & Peng, S. G. Development of measuring diffusion coefficients by digital holographic interferometry in transparent liquid mixtures. *Opt. Express* **23**, 10884 (2015).